The Full Strength of Cluster Gravitational Lensing:

Mass Distribution in and around Cosmic Giants from the CLASH Survey

Cluster Lensing And Supernova survey with Hubble

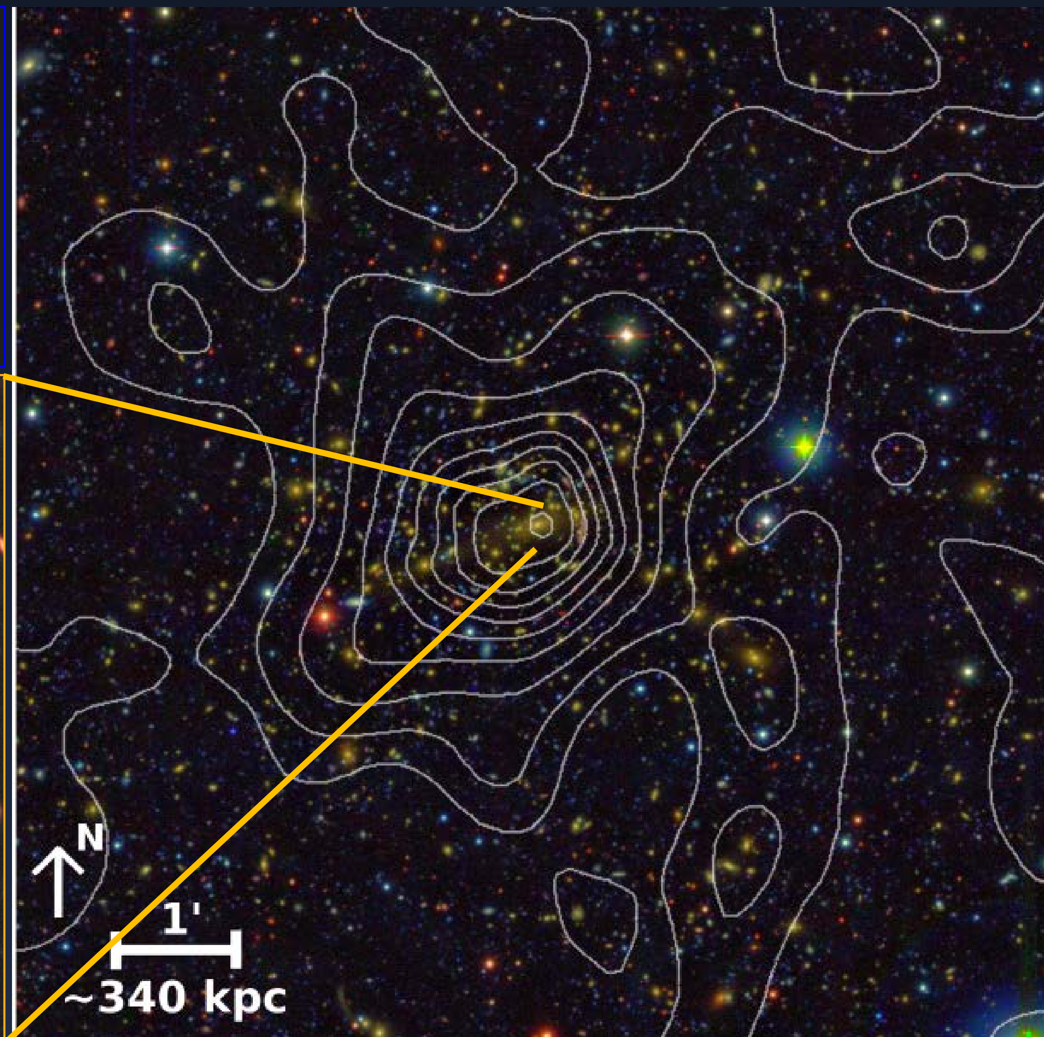

Keiichi Umetsu (ASIAA, Taiwan)

Contents

1. Introduction

Galaxy Clusters as Cosmological Probe

Clusters of Galaxies

Strong and weak lensing

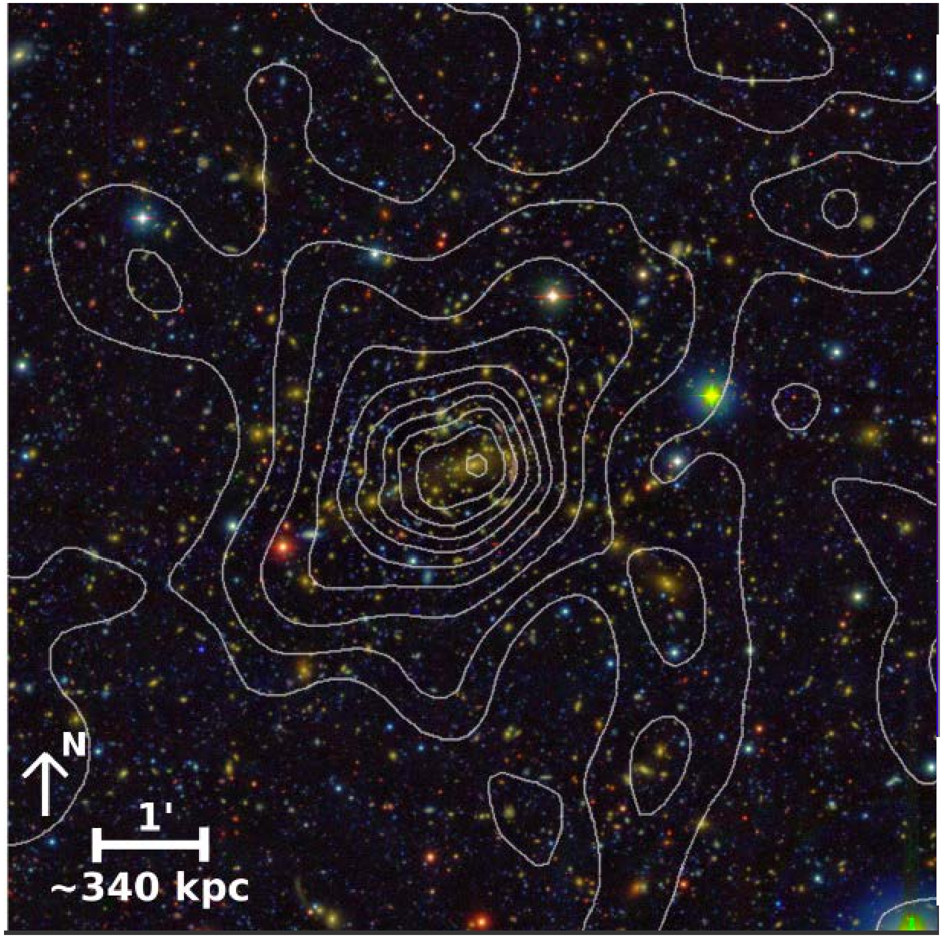

Sunyaev-Zel'dovich Effect (SZE)

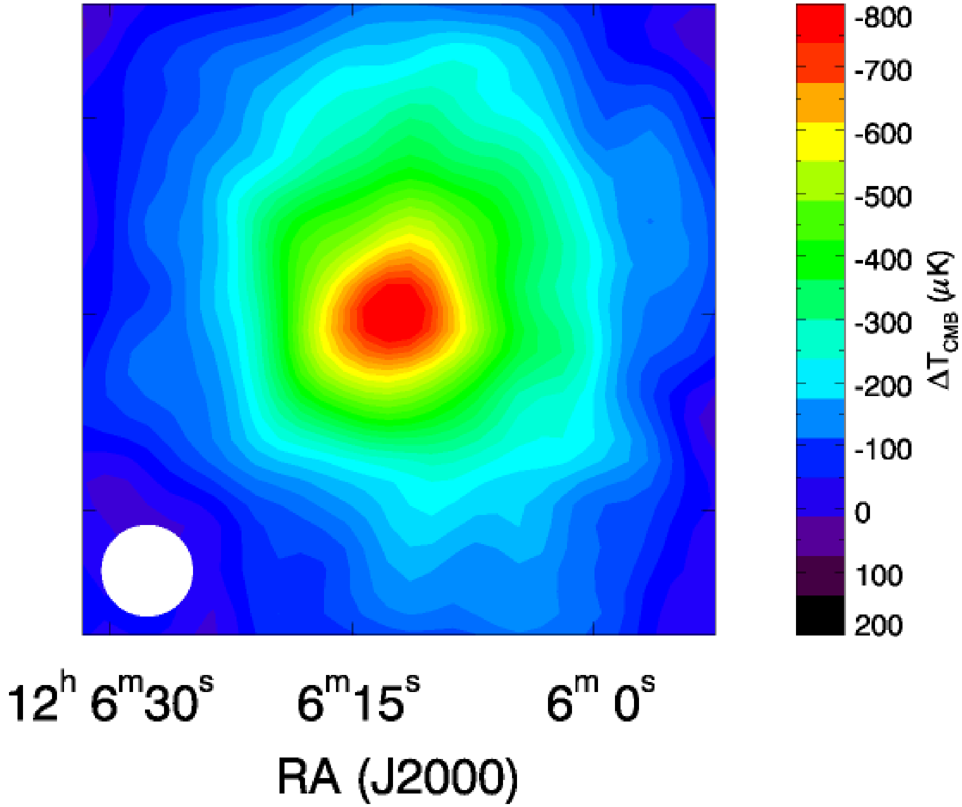

MACS1206 cluster at z=0.44
(Umetsu et al. 2012, *ApJ*, 755, 56)

Clusters: the largest/rarest class of DM halos

Halos = gravitationally-bound objects $\frac{1}{2}\ddot{I} = 2K + U - E^{(S)} \sim 0$

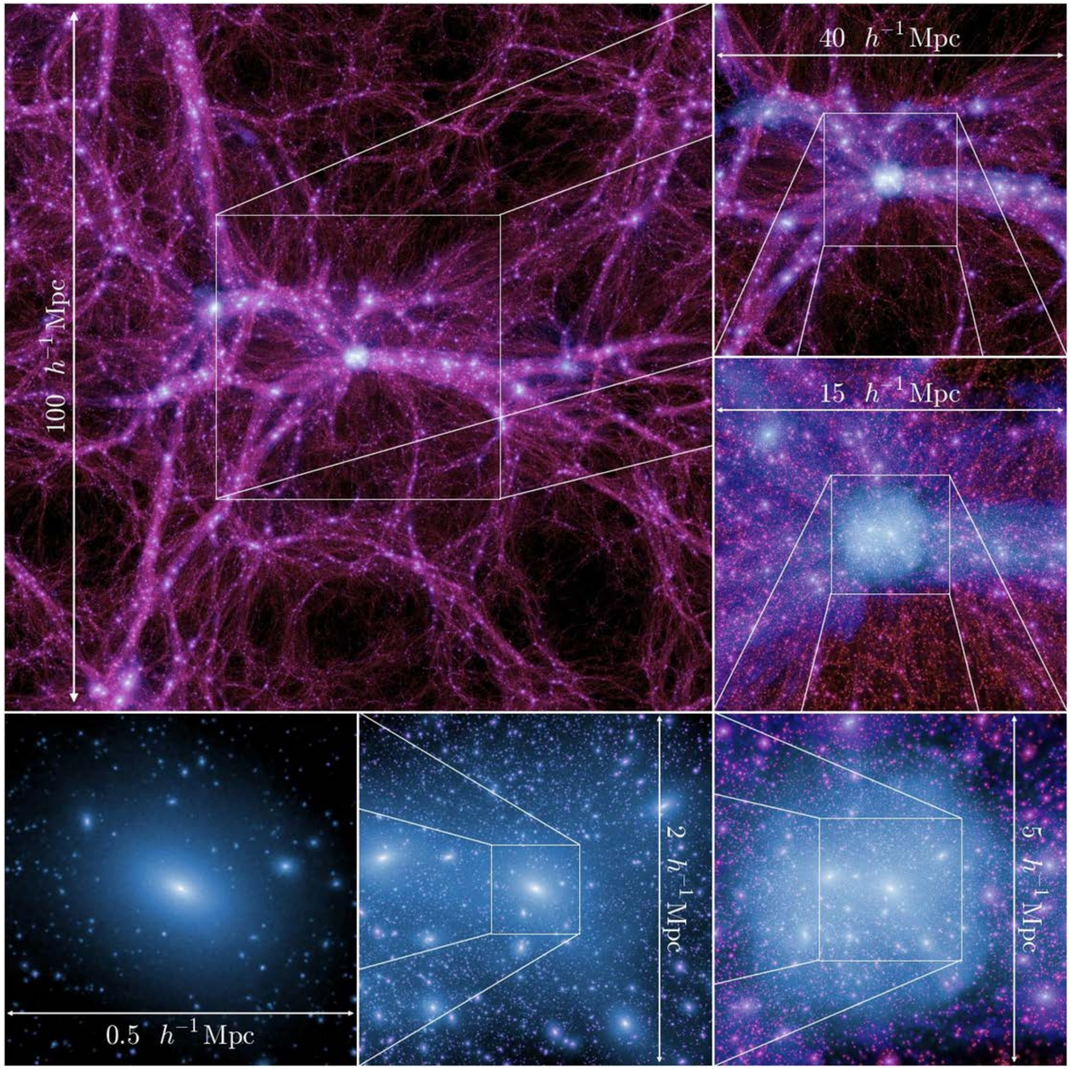

Clusters formed at the intersection of filaments and sheets

Typical formation epoch: z_f=0.5-0.7

Young halos are prolate (collisionless nature)

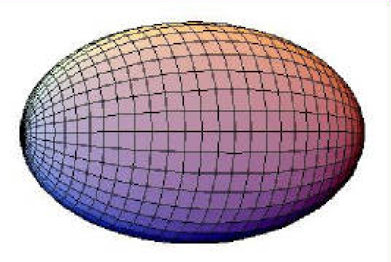

Boylan-Kolchin+09

Clusters as Cosmological Probe

Cluster counts $$\frac{dN(>M_{\lim},z)}{d\Omega dz} = \int_{M_{\lim}}^{\infty} dM \frac{dV(z)}{d\Omega dz} \frac{d^2 n}{dVdM}(M,z)$$

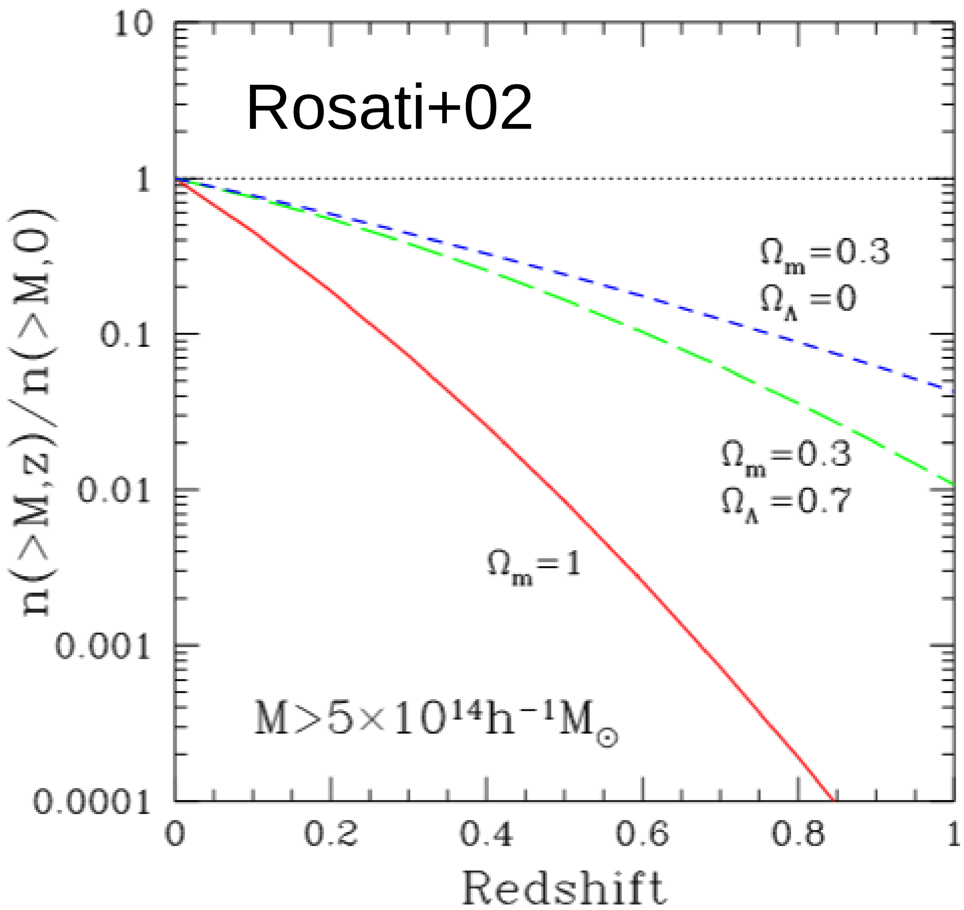

Comoving volume element

$$\frac{d^2V}{dzd\Omega} = \frac{cr^2[\chi(z)]}{H(z)}, \quad \chi(z) = \int_0^z \frac{dz'}{H(z')}$$

Halo mass function

$$\frac{d^2 n}{dVdM}(M,z) \propto \exp\left[-\frac{\nu^2}{2}\right]$$

$$\nu \equiv \frac{\delta_c(z)}{\sigma(M,z)} \approx \frac{1.69}{D_+(z)\sigma(M)} \sim 3 \text{ for clusters}$$

Cluster counts are exponentially sensitive to *cosmology* and ***cluster mass calibration***!

Key Predictions of nonlinear structure formation models

(1) Quasi self-similar DM-halo density profiles

Quasi self-similar DM halo density profiles

Spherically-averaged density profiles $\rho_h(r)$ of collisionless DM halos from numerical simulations $\rho_h(r) \sim \rho_s f(r/r_s)$

Cuspy, outwardly-steepening density profiles

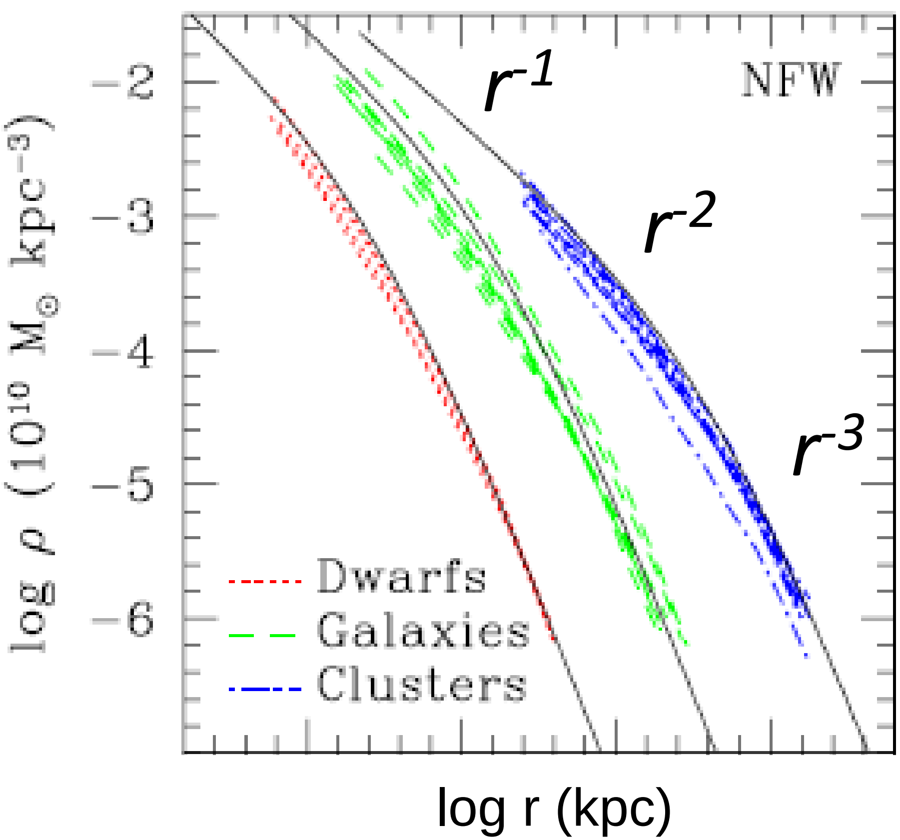

Theoretical models:

- **DARKexp** (Hjorth & Williams 10): Statistical mechanical arguments to describe the distribution of particle energies in finite, self-gravitating, collisionless systems, providing theoretical predictions for the structure of collisionless DM halos.
- Pontzen & Governato 13: Maximum-entropy arguments to derive the phase-space distribution for an end product of violent relaxation
- Adhikari, Dalal, & Chamberlain 14: outskirt steepening associated with first apocentric passage after accretion

Key Predictions of nonlinear structure formation models

(2) Halo concentration-mass relation

Degree of Mass Concentration

$$c_{200} \equiv \frac{r_{200}}{r_s} = \frac{\text{(Outer scale radius)}}{\text{(Inner scale radius)}}$$

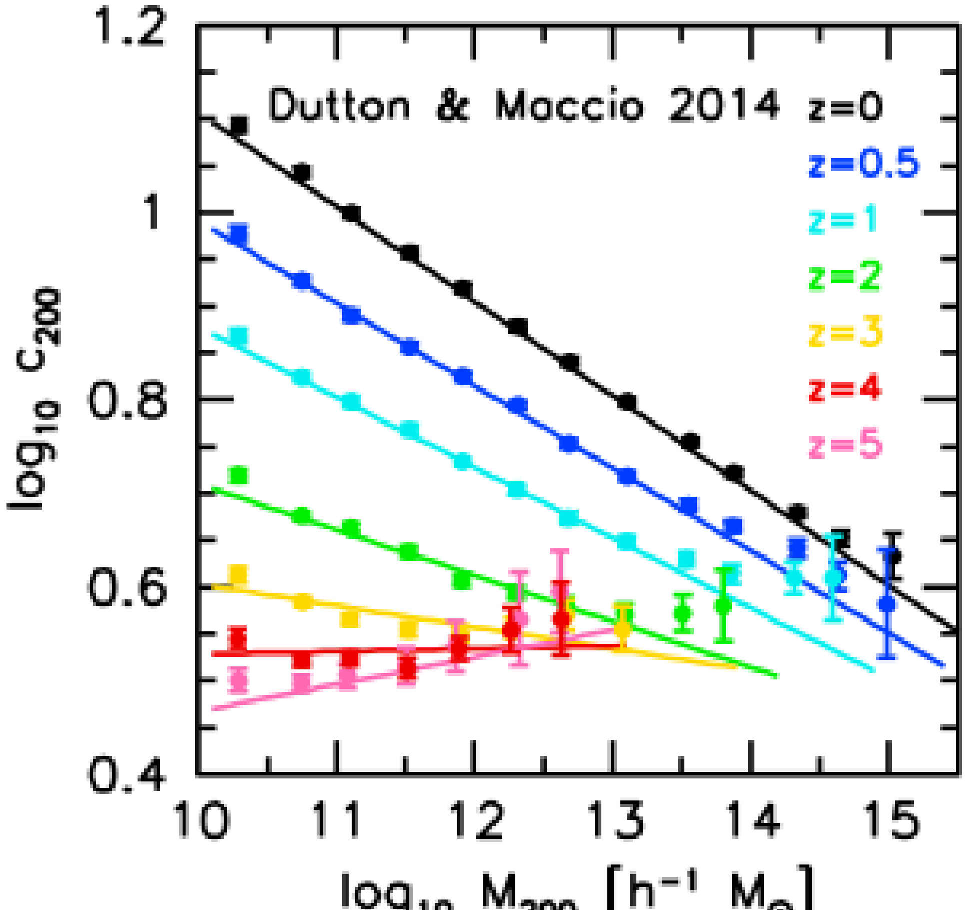

In hierarchical structure formation, <*c*> is predicted to correlate with *M*

DM halos that are more massive collapse later on average, when the mean background density of the universe is correspondingly lower (e.g., Bullock+01)

Concentration is sensitive to cosmology

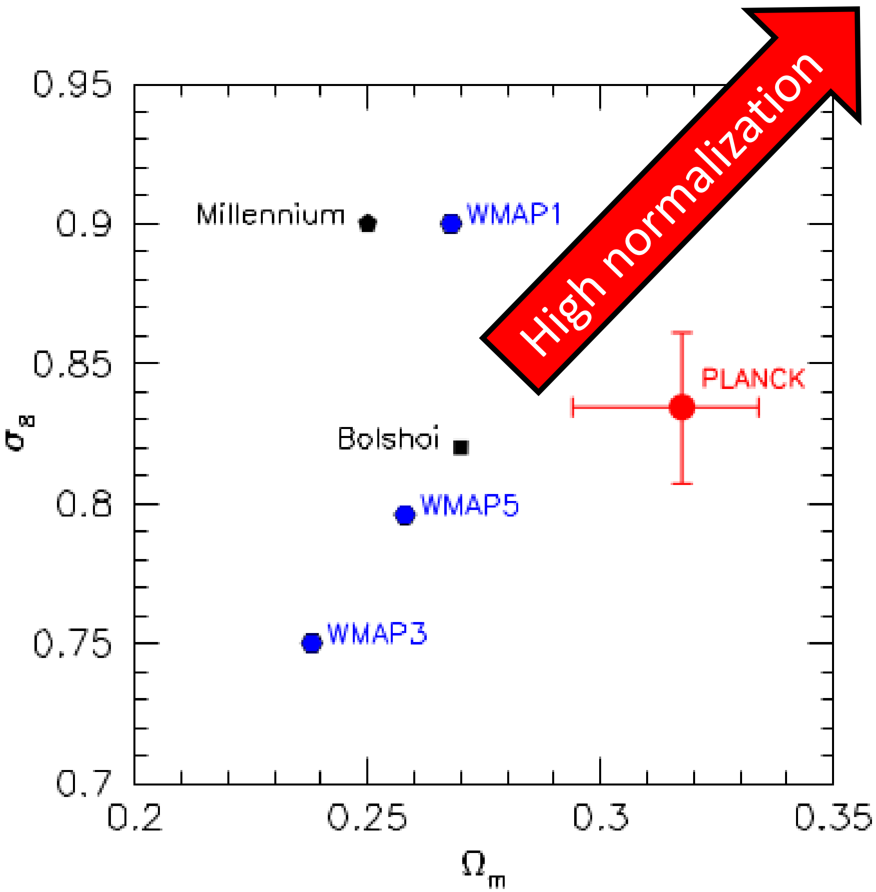

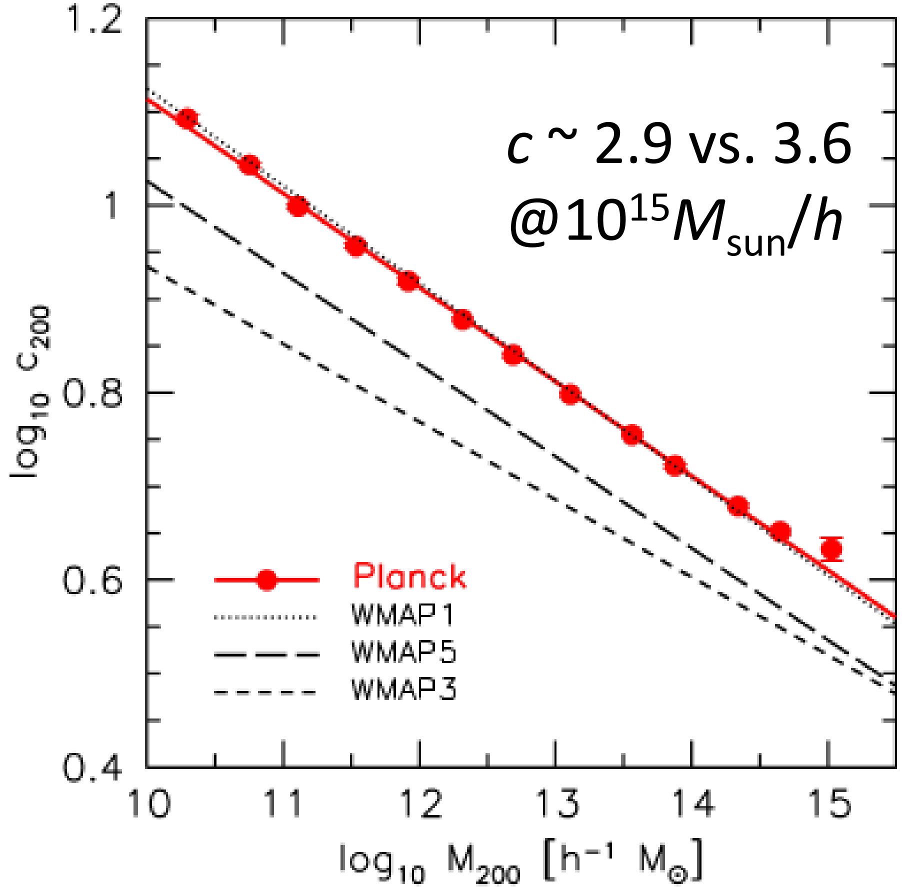

Dutton & Maccio 2014

Intrinsic Scatter in $c(M)$: Mass Assembly Histories (MAH)

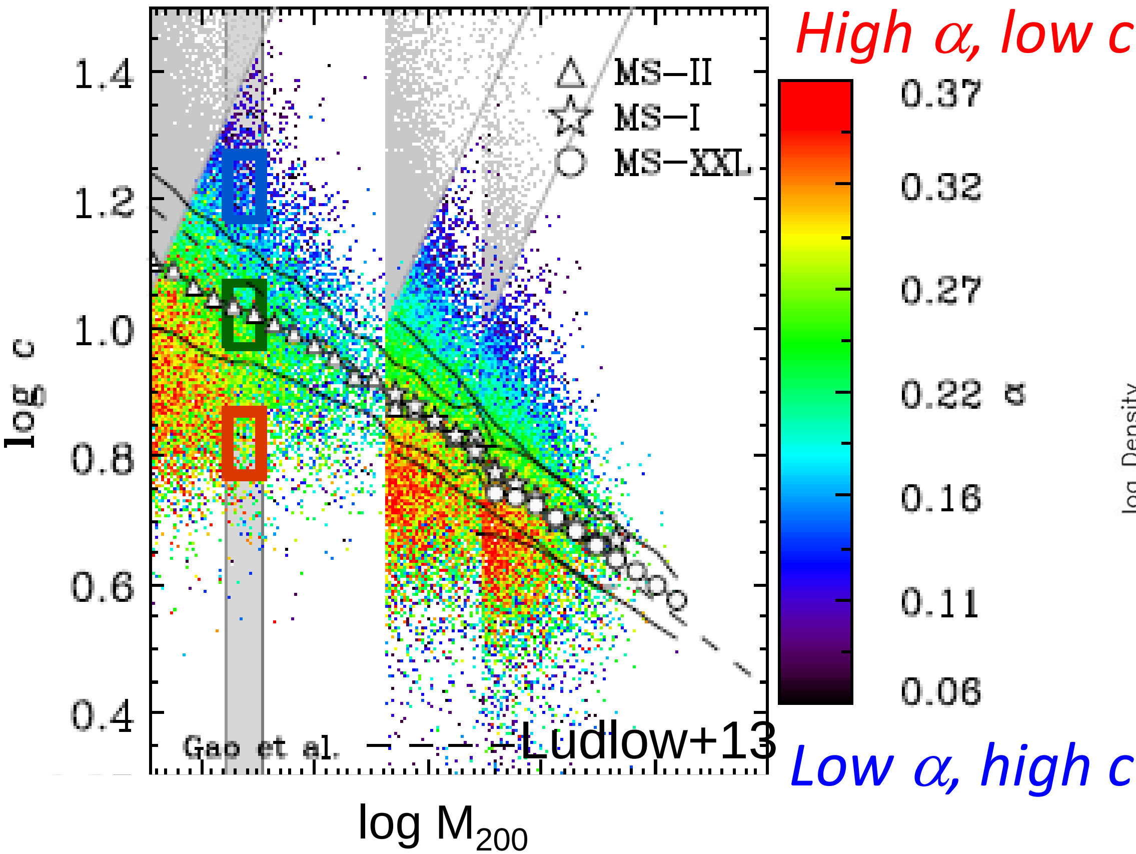

α: degree of curvature

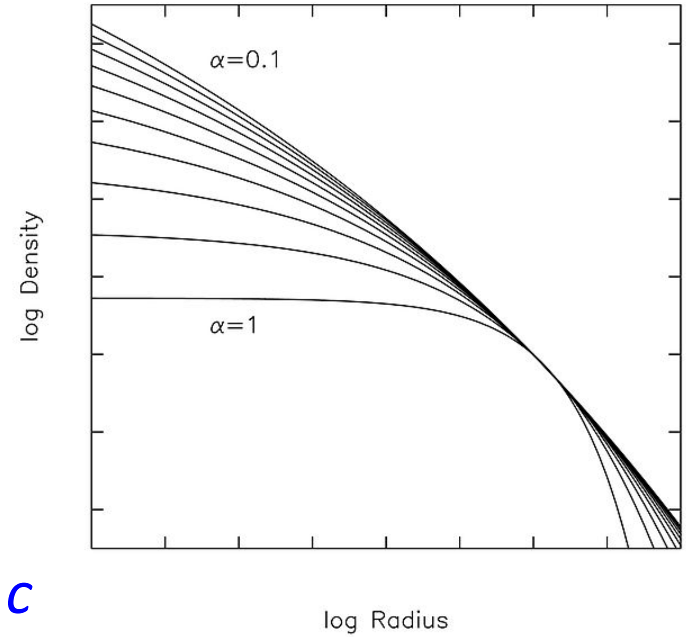

- Scatter is due to another DoF (α), related to MAH (Ludlow+13)
- Larger values of α correspond to halos that have been assembled more rapidly than the NFW curve
- Halos with average c_{200} have the NFW-equivalent α ~0.18

Key Predictions of nonlinear structure formation models

(3) Halo bias: surrounding large-scale structure

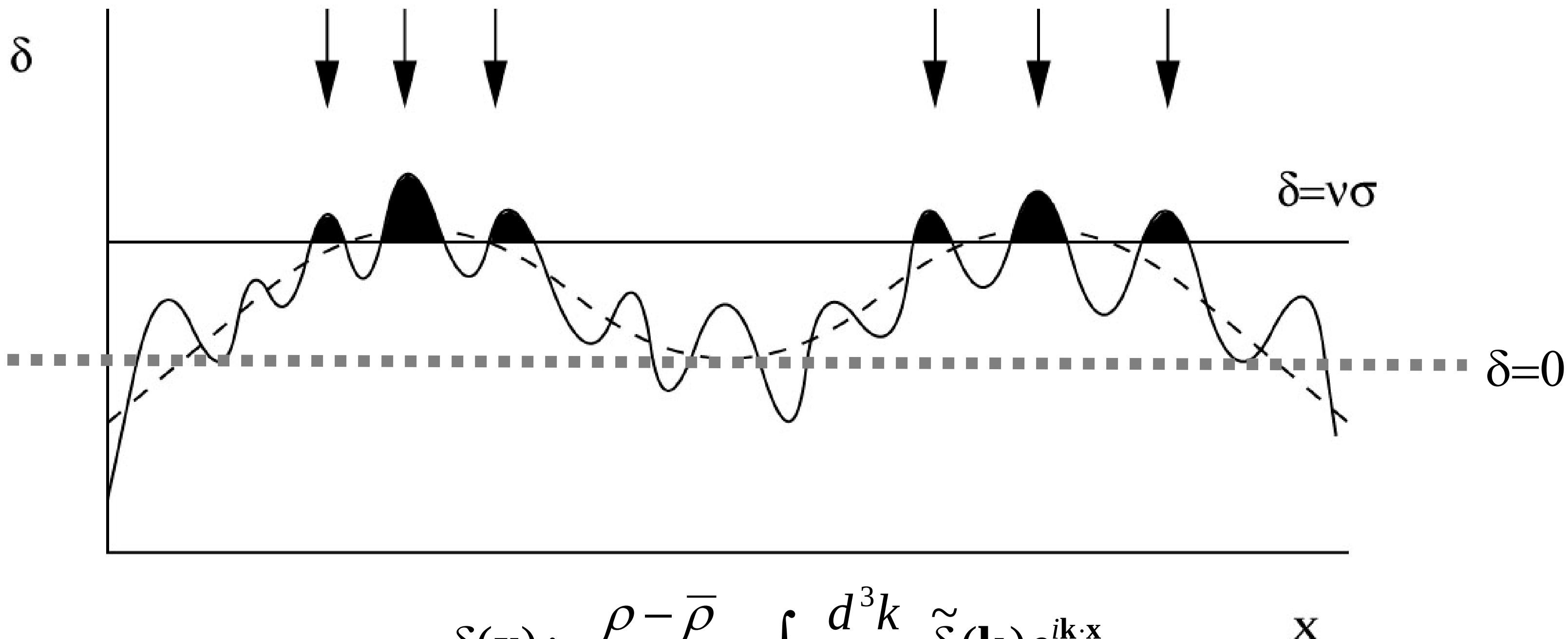

$$\delta(\mathbf{x}) := \frac{\rho - \bar{\rho}}{\bar{\rho}} = \int \frac{d^3k}{(2\pi)^3} \tilde{\delta}(\mathbf{k}) e^{i\mathbf{k}\cdot\mathbf{x}}$$

$$\left\langle \tilde{\delta}(\mathbf{k}) \tilde{\delta}(\mathbf{k}') \right\rangle = (2\pi)^3 \delta_D^3(\mathbf{k} + \mathbf{k}') P(k)$$

Halo Bias Factor: b_h

Clustering of matter around halos with *M*:

$$\xi_{\rm hm}(r\,|\,M) \equiv \left\langle \delta_{\rm h}(\mathbf{x}\,|\,M)\delta_{\rm m}(\mathbf{x}+\mathbf{r})\right\rangle$$

$$= \frac{\left\langle \rho_{\rm h}(r\,|\,M)\right\rangle}{\bar{\rho}} + b_{\rm h}(M)\xi_{\rm mm}(r)$$ **2h term**

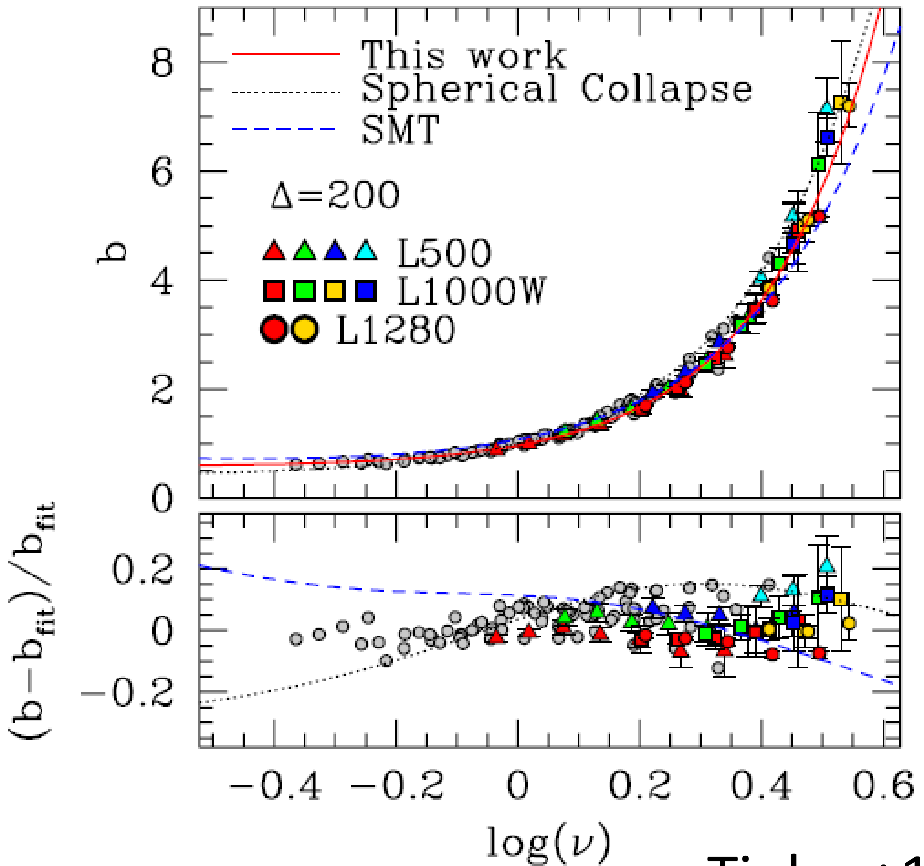

Correlated matter distribution (2h term)

Matter correlation function:

$$\xi_{\rm mm}(\mathbf{r}) \equiv \left\langle \delta_{\rm m}(\mathbf{x})\delta_{\rm m}(\mathbf{x}+\mathbf{r})\right\rangle = \int \frac{d^3k}{(2\pi)^3} P(k) e^{i\mathbf{k}\cdot\mathbf{r}}$$

$$\propto \sigma_8^2$$

Linear halo bias:

$$b_{\rm h}(\nu) \approx 1 + \frac{\nu^2 - 1}{\delta_c}$$

$$\nu \equiv \frac{\delta_c}{\sigma(M,z)} \sim 3-4 \text{ for clusters}$$

Tinker+10 LCDM simulations

2. Cluster Gravitational Lensing

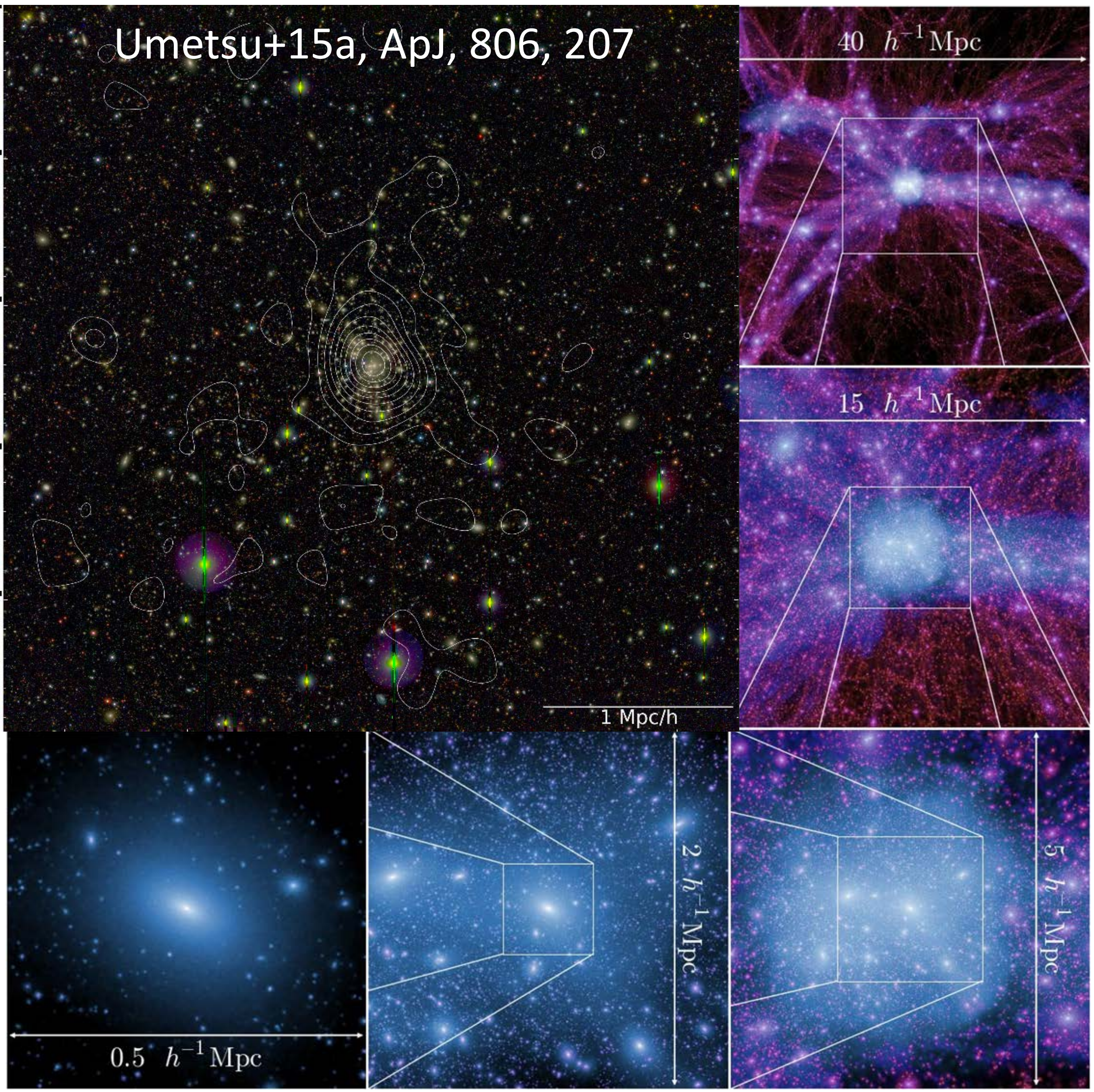

Key Objectives

Cluster structure (1h)

Halo mass, M

Halo density profile, $\rho(r)$

c-M relation, c(M,z)

Surrounding LSS (2h)

Halo bias $b_h(M,z)$

Clustering strength σ_8

Multiple Imaging (Strong Lensing)

$$\alpha = \partial\Psi$$

$$\partial := \partial_x + i\partial_y = e^{i\phi}\partial_r$$

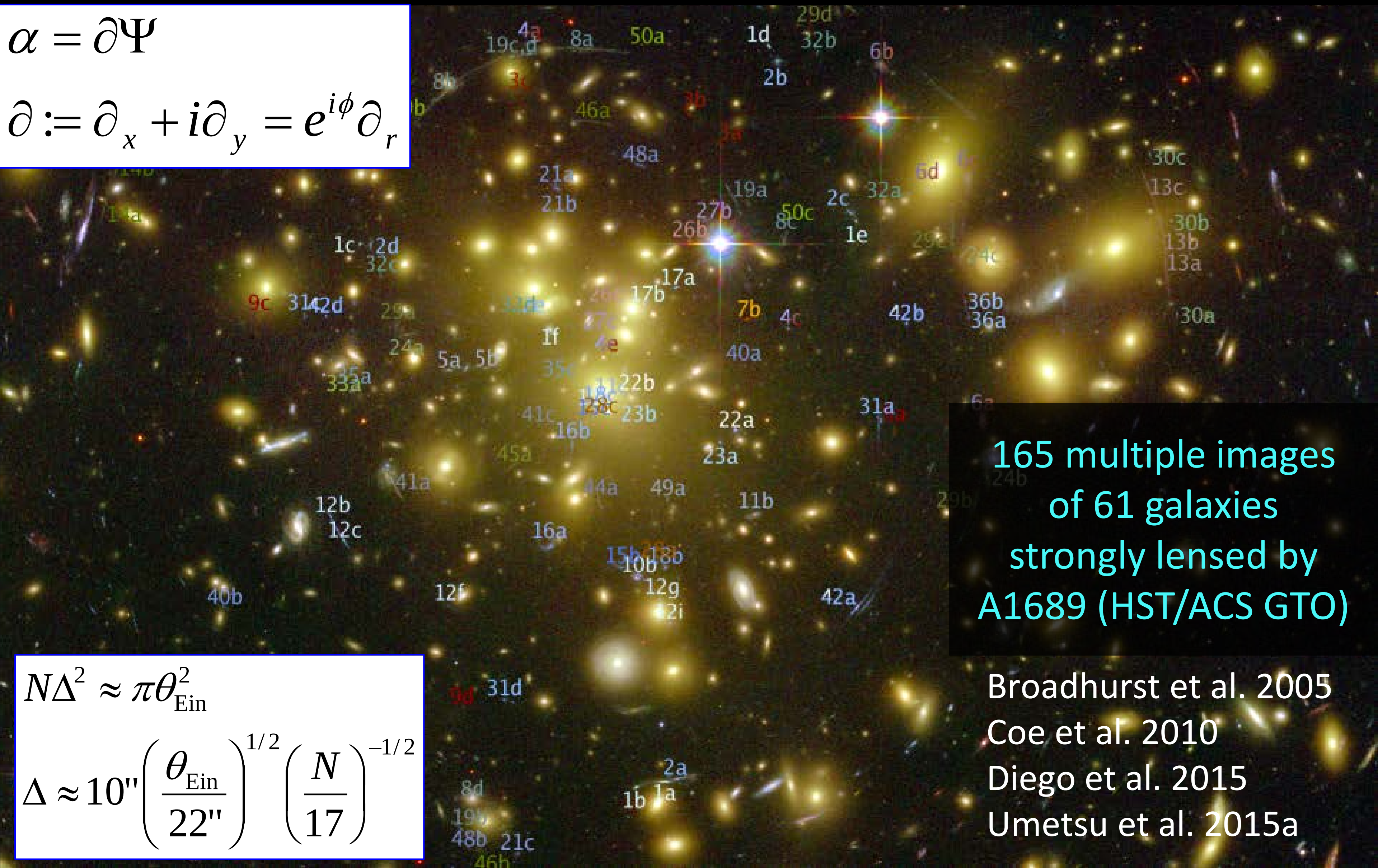

165 multiple images of 61 galaxies strongly lensed by A1689 (HST/ACS GTO)

$$N\Delta^2 \approx \pi\theta_{\rm Ein}^2$$

$$\Delta \approx 10''\left(\frac{\theta_{\rm Ein}}{22''}\right)^{1/2}\left(\frac{N}{17}\right)^{-1/2}$$

Broadhurst et al. 2005
Coe et al. 2010
Diego et al. 2015
Umetsu et al. 2015a

Gravitational Shear

$$\gamma = \partial\partial\Psi / 2$$

$$\partial := \partial_x + i\partial_y = e^{i\phi}\partial_r$$

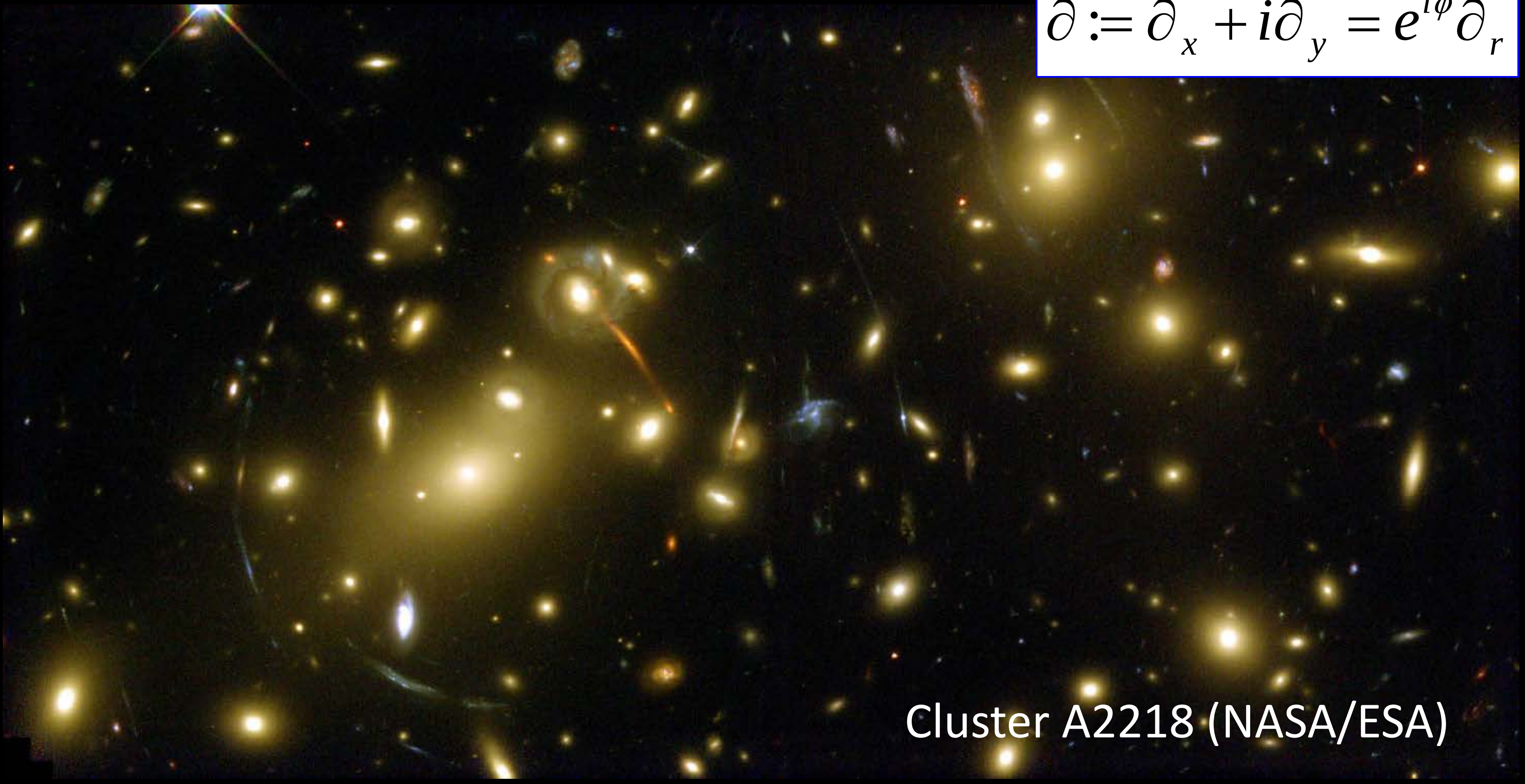

Cluster A2218 (NASA/ESA)

Gravitational Magnification

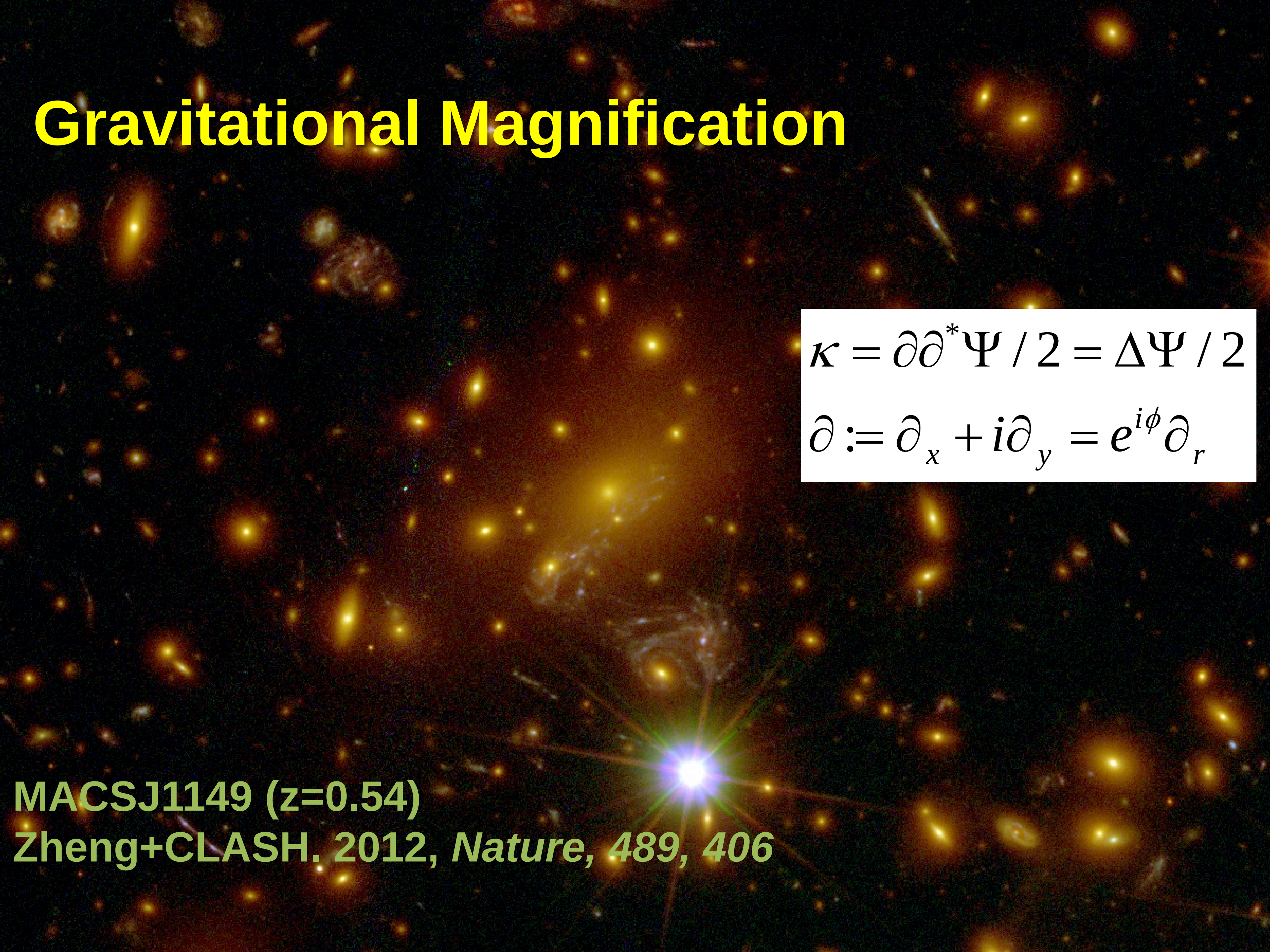

$$\kappa = \partial\partial^{*}\Psi / 2 = \Delta\Psi / 2$$

$$\partial := \partial_x + i\partial_y = e^{i\phi}\partial_r$$

MACSJ1149 (z=0.54)

Zheng+CLASH. 2012, *Nature, 489, 406*

Shear and Magnification Effects

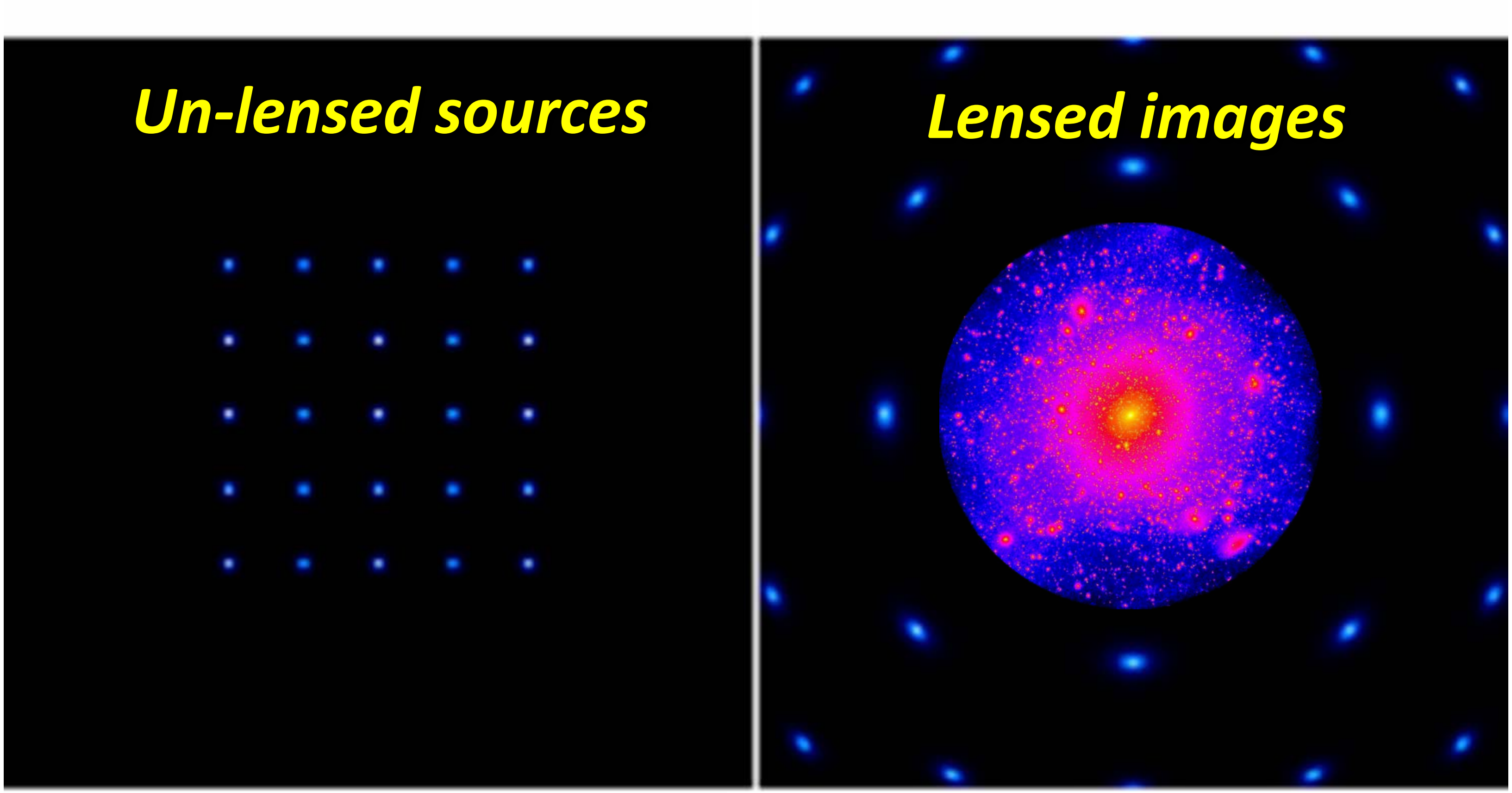

- **Shear**
  - ✓ Shape distortion: $\delta e_+ \sim \gamma_+$
- **Magnification**
  - ✓ Flux amplification: μF
  - ✓ Area distortion: $\mu \Delta \Omega$

Sensitive to "modulated" matter density

$$\Sigma_c \gamma_+ = \Delta\Sigma(R) \equiv \Sigma(<R) - \Sigma(R)$$

Sensitive to "total" matter density

$$\mu \approx 1 + 2\kappa; \quad \Sigma_c \kappa = \Sigma(R)$$

Tangential Shear, γ_+

A measure of azimuthally-averaged tangential coherence of elliptical distortions around a given point (Kaiser 95):

$$\gamma_+(R) = \Delta\Sigma(\mathrm{R}) / \Sigma_{\mathrm{c}}$$

$$(\boldsymbol{\Gamma}_+)_{ij} = \left(\boldsymbol{\delta}_i\boldsymbol{\delta}_j - \frac{\mathbf{1}}{\mathbf{2}}\Delta^{(2)}\boldsymbol{\delta}_{ij}\right)\boldsymbol{\psi}_+$$

$$\gamma_\times(R) = 0$$

$$(\boldsymbol{\Gamma}_X)_{ij} = (\boldsymbol{\epsilon}_{kj}\boldsymbol{\partial}_i\boldsymbol{\partial}_k - \boldsymbol{\epsilon}_{ki}\boldsymbol{\partial}_j\boldsymbol{\partial}_k)\boldsymbol{\psi}_X$$

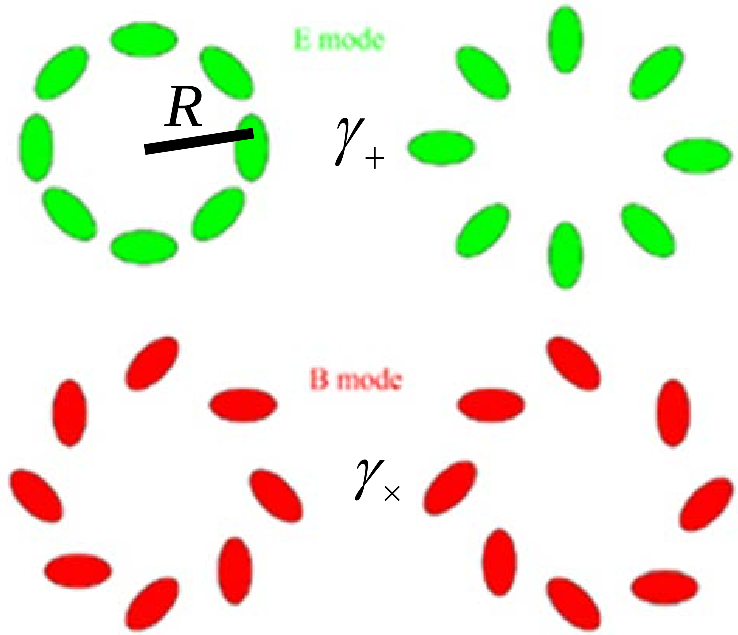

ΔΣ(*R*) is radially-*modulated* surface mass density:

$$\Delta\Sigma(R) = \Sigma(< R) - \Sigma(R)$$

Sensitive to interior mass

$$\Sigma(R) = \int dl\, \Delta\rho(r),$$

$$\Sigma_{\mathrm{c}} = \frac{c^2}{4\pi G}\frac{D_{\mathrm{S}}}{D_{\mathrm{L}} D_{\mathrm{LS}}}$$

Shear doesn't see mass sheet

Averaged lensing profiles in/around LCDM halos (Oguri & Hamana 11)

Total

$$\kappa = \Sigma(R) / \Sigma_c$$

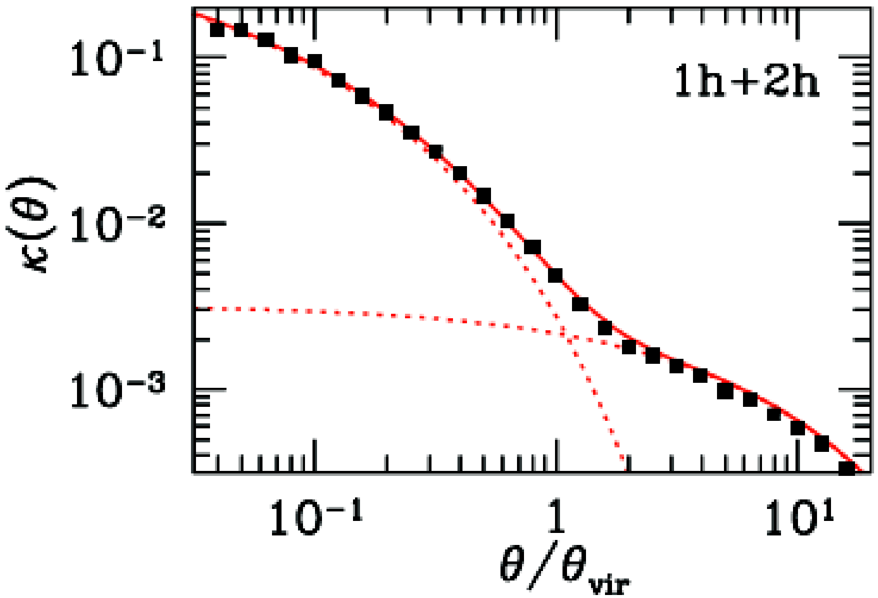

Modulated

$$\gamma_+ = \Delta\Sigma(R) / \Sigma_c$$

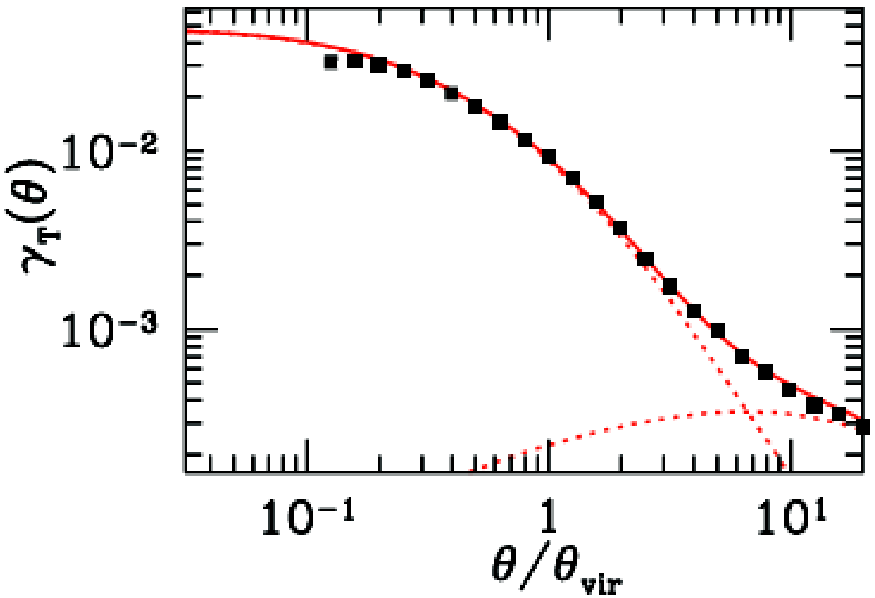

- **Tangential shear is a powerful probe of 1-halo term, or internal halo structure.**
- **Shear alone cannot recover absolute mass, known as *mass-sheet degeneracy:***

γ remains unchanged by $\kappa \rightarrow \kappa + \text{const.}$

Non-local substructure effect

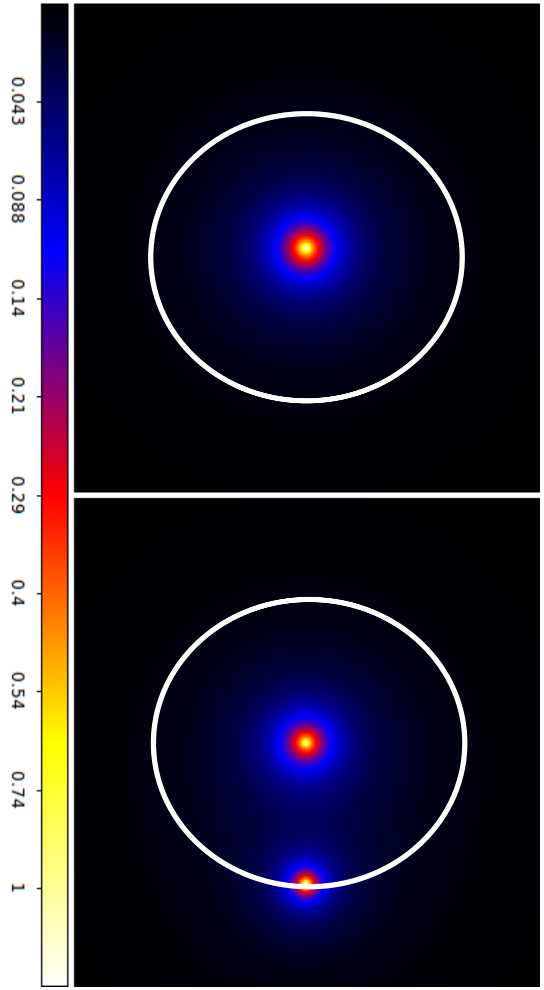

A substructure at $R \sim r_{\rm vir}$ of the main halo, modulating $\Delta\Sigma(R) = \Sigma(<R) - \Sigma(R)$

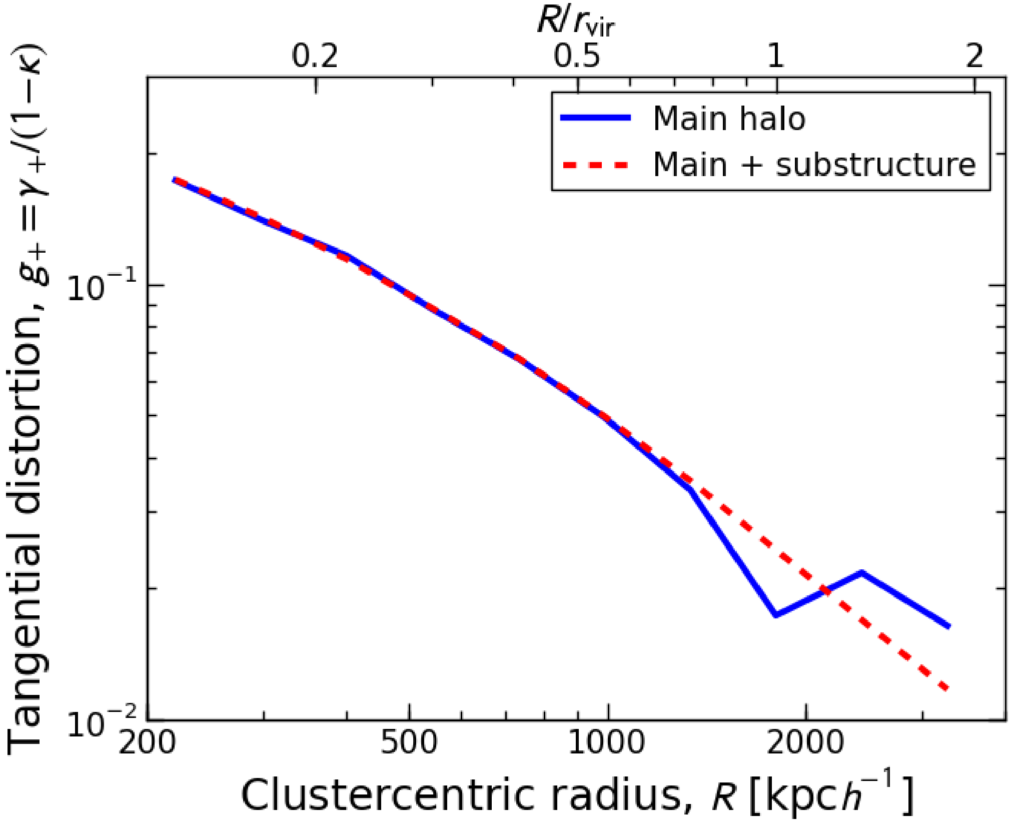

Known 5%-10% negative bias in mass estimates from tangential-shear fitting, inherent to rich substrucure in outskirts (Rasia+12)

Magnification bias effects

Flux-limited source counts:

$$n_{\mathrm{obs}}(>f) = \mu^{-1} n(>\mu^{-1} f)$$

Broadhurst, Taylor & Peacock 1995

Geometric area distortion

n/μ

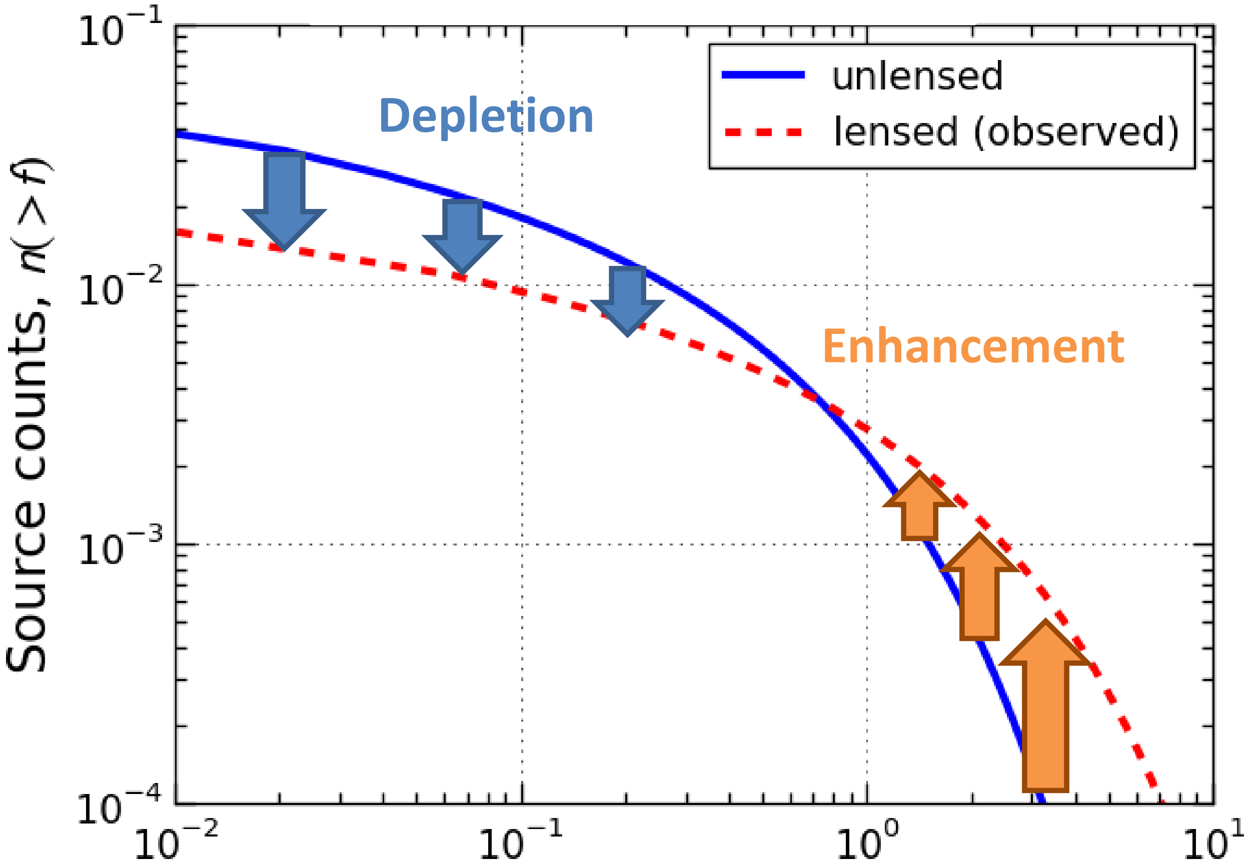

Flux amplification

Negative Magnification Bias

Depletion of Number Counts

Geometric shear-magnification consistency

Deep counts of red quiescent galaxies at <z>~1 are highly depleted

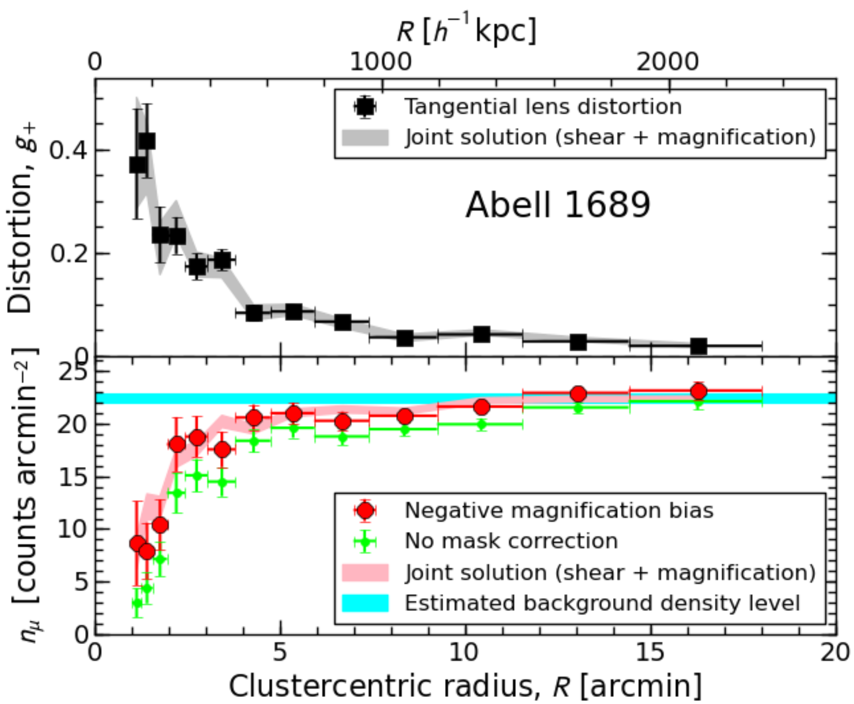

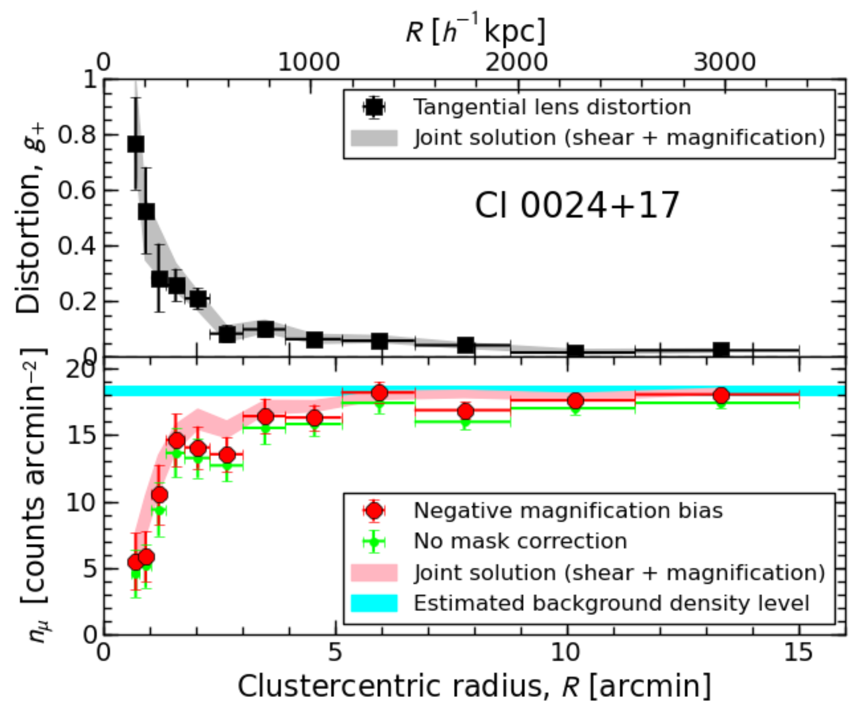

Subaru/Suprime-Cam data

Umetsu et al. 2011a, ApJ, 729, 127

Combining Shear and Magnification

Joint likelihood approach

$$L(\boldsymbol{\kappa}) = L_g(\boldsymbol{\kappa} \mid \mathbf{g}_+) L_\mu(\boldsymbol{\kappa} \mid \boldsymbol{\mu})$$

Tangential distortion

$$g_+(R) = \frac{\kappa(<R) - \kappa(R)}{1 - \kappa(R)},$$

Inverse magnification

$$\mu^{-1}(R) = [1 - \kappa(R)]^2 - [\kappa(<R) - \kappa(R)]^2$$

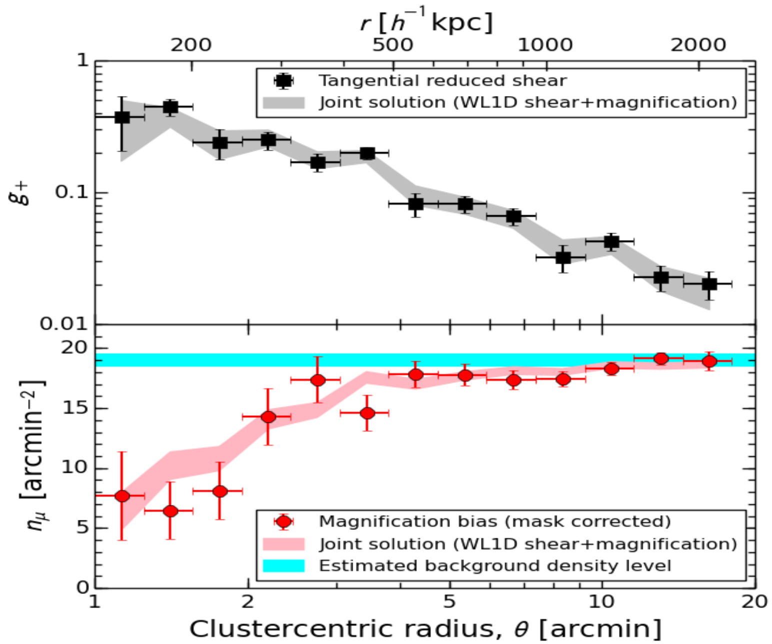

g_+

μ^{-1}

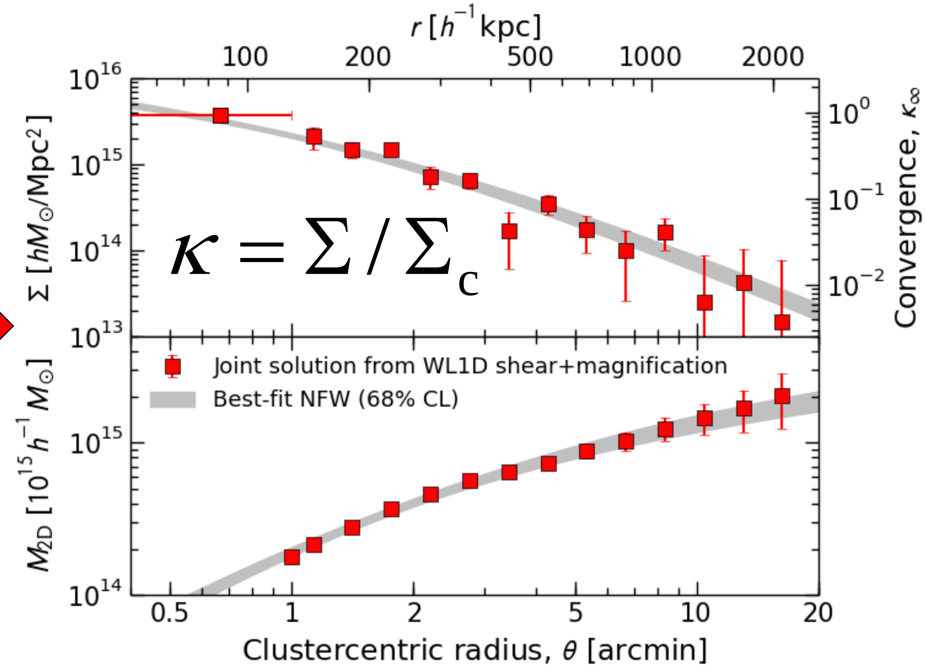

- Mass-sheet degeneracy broken
- Total statistical precision improved by ~20-30%
- Calibration uncertainties marginalized over: $c = \{\langle W\rangle_s, f_{W,s}, \langle W\rangle_\mu, \overline{n}_\mu, s_{\rm eff}\}$.

Multi-probe Lensing Approach:

Combining azimuthally-averaged lensing observables

$$\{M_{2\mathrm{D},i}\}_{i=1}^{N_{\mathrm{SL}}}, \{\langle g_{+,i}\rangle\}_{i=1}^{N_{\mathrm{WL}}}, \{\langle n_{\mu,i}\rangle\}_{i=1}^{N_{\mathrm{WL}}}.$$

$$L(\boldsymbol{\kappa}) = L_{\mathrm{SL}}(\boldsymbol{\kappa}\,|\,\mathbf{M}_{\mathbf{2D}})L_g(\boldsymbol{\kappa}\,|\,\mathbf{g}_+)L_\mu(\boldsymbol{\kappa}\,|\,\boldsymbol{\mu})$$

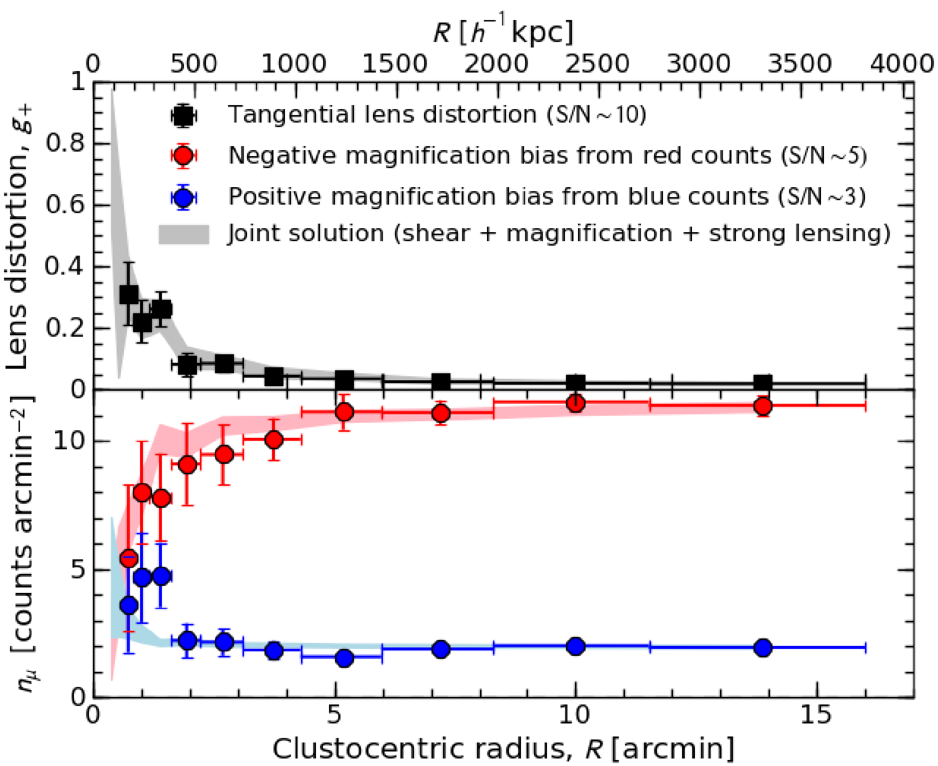

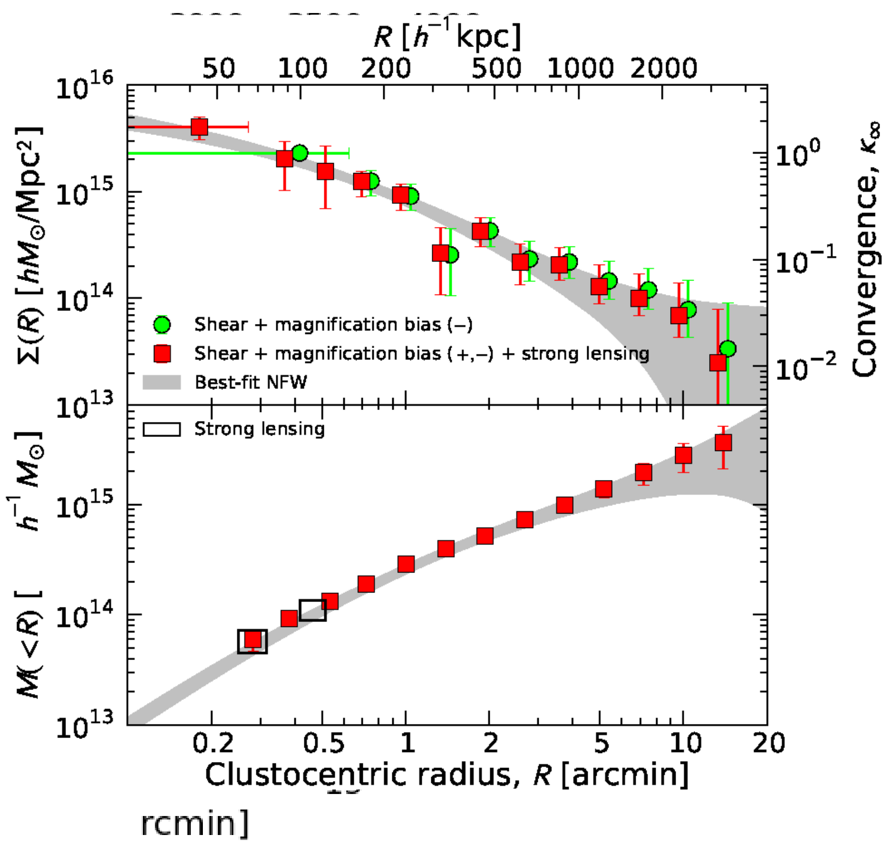

Umetsu 2013, ApJ, 769, 13

Cluster Lensing And Supernova survey with Hubble

CLASH

PI. Marc Postman (STScI)

http://www.stsci.edu/~postman/CLASH/Home.html

CLASH Objectives & Motivation

Before CLASH (2010), deep-multicolor Strong (*HST*) + Weak (*Subaru*) lensing data only available for a handful of “**super lens” clusters**

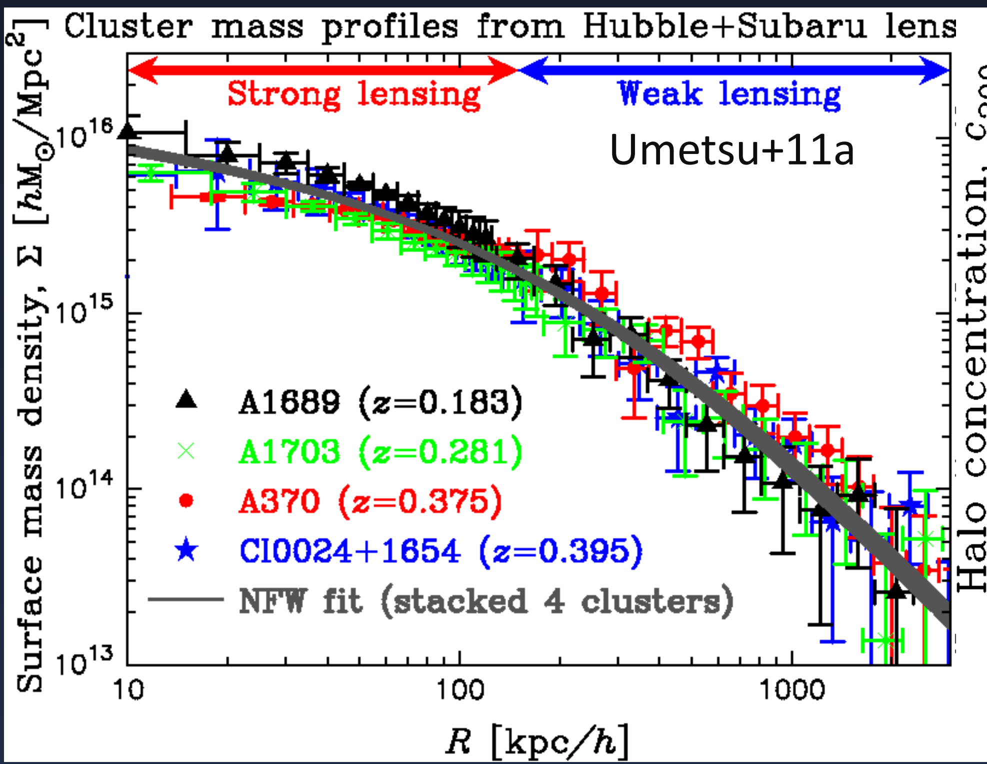

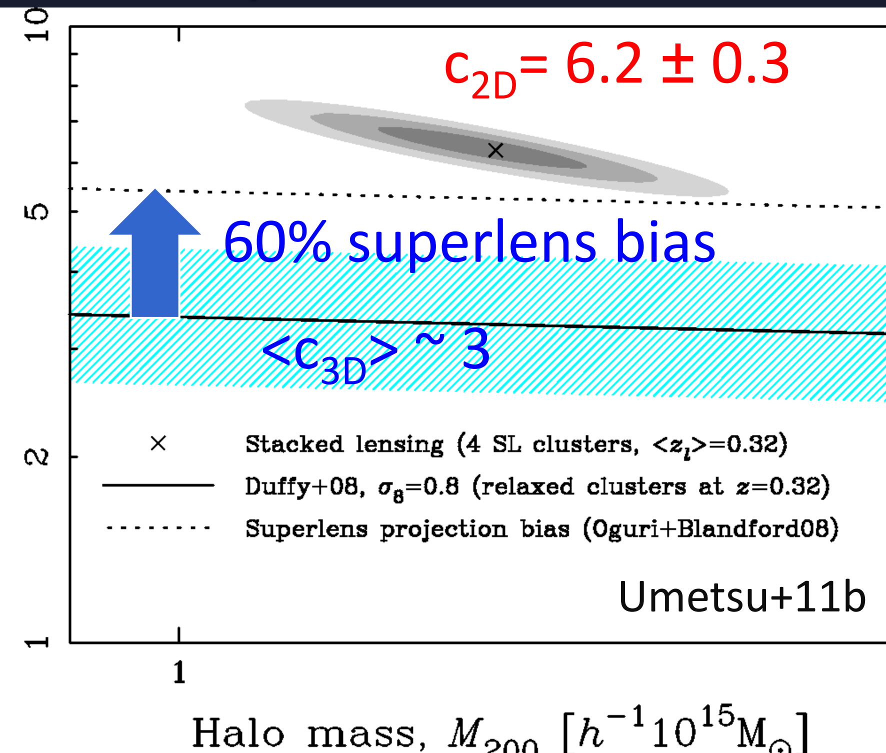

Total mass profile shape: consistent w self-similar NFW (cf. Newman+13; Okabe+13)

Degree of concentration: predicted superlens correction not enough if $<c_{LCDM}>$~3?

CLASH Objectives & Motivation

Before CLASH (2010), deep-multicolor Strong (*HST*) + Weak (*Subaru*) lensing data only available for a handful of "**super lens" clusters**

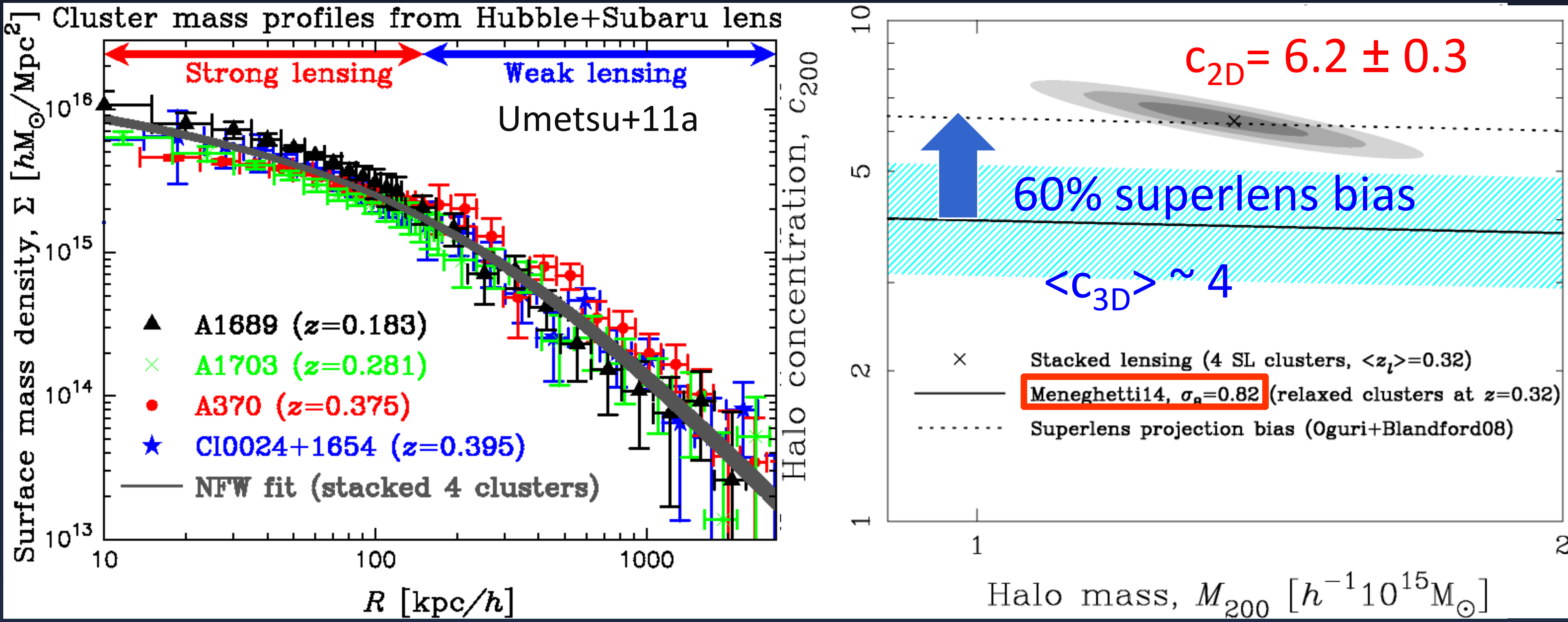

Total mass profile shape: consistent w self-similar NFW (cf. Newman+13; Okabe+13)
Degree of concentration: predicted superlens correction is just enough if $<c_{LCDM}>\sim4$

CLASH: Observational + Theory Efforts

A 524-orbit *Hubble* Treasury Program to observe 25 clusters in 16 filters (0.23-1.6 μm) (Postman et al. 2012)

Wide-field Subaru imaging (0.4 - 0.9 μm) plays a unique role in complementing deep *HST* imaging of cluster cores (Umetsu et al. 2014, *ApJ*, 795, 163)

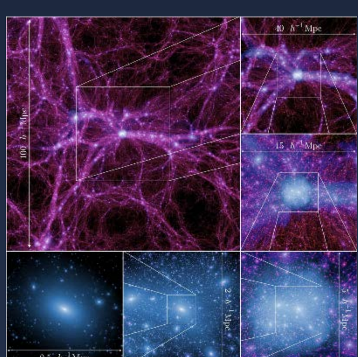

MUSIC-2 (hydro + N-body re-simulation) provides an accurate characterization of CLASH sample with testable predictions (Meneghetti et al. 2014, *ApJ*, 797, 34)

SUBARU (S-Cam) multi-color imaging for wide-field weak

High-resolution space imaging with *HST* (ACS/WFC3) for strong lensing

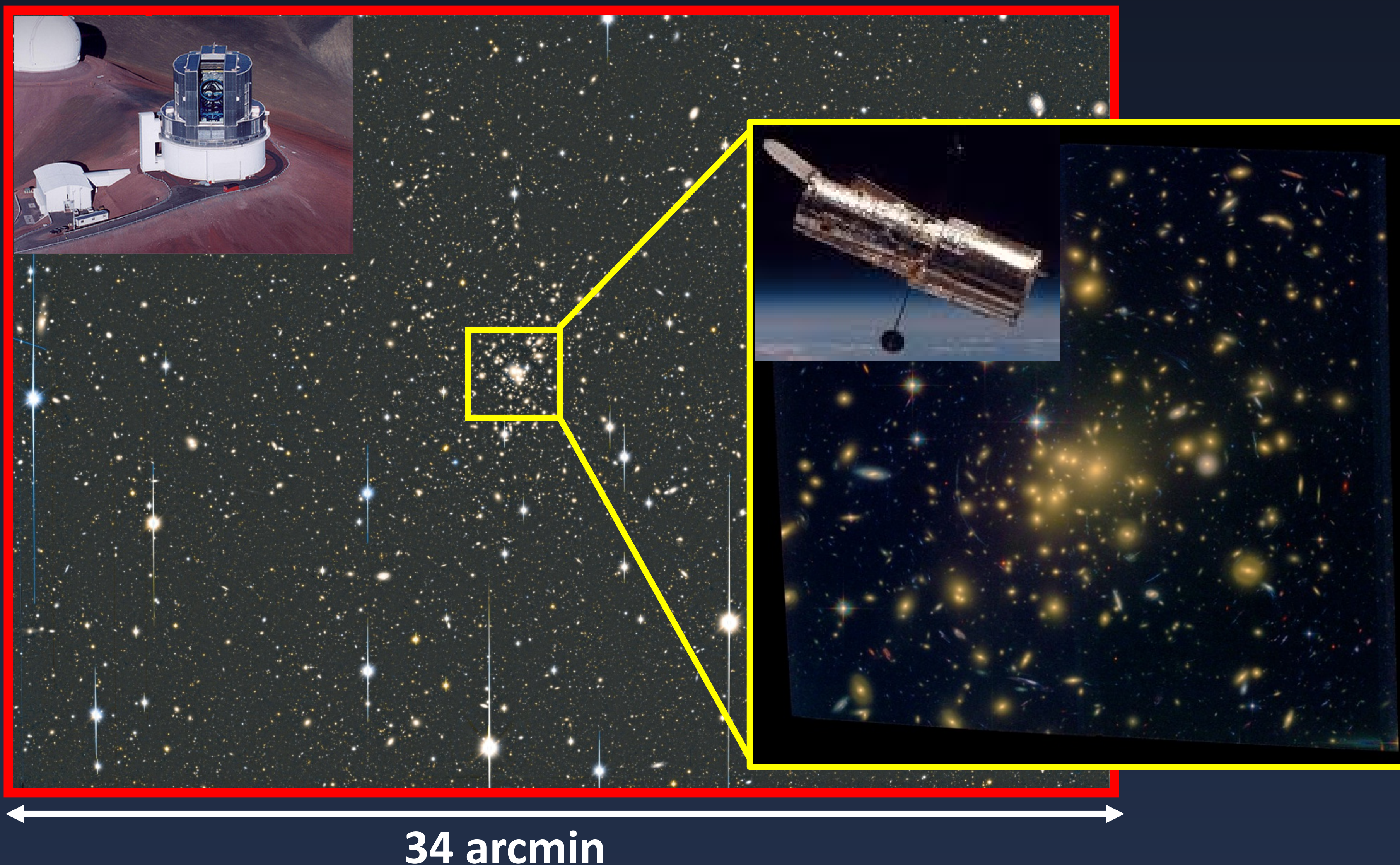

CLASH *HST* Dataset

The final HST observation for CLASH was on 9-July-2013 ··· 963 days, 15 hrs, 31 min after first obs.

Zitrin et al. 2015, *ApJ*, 801, 44

Subaru Weak-lensing Dataset

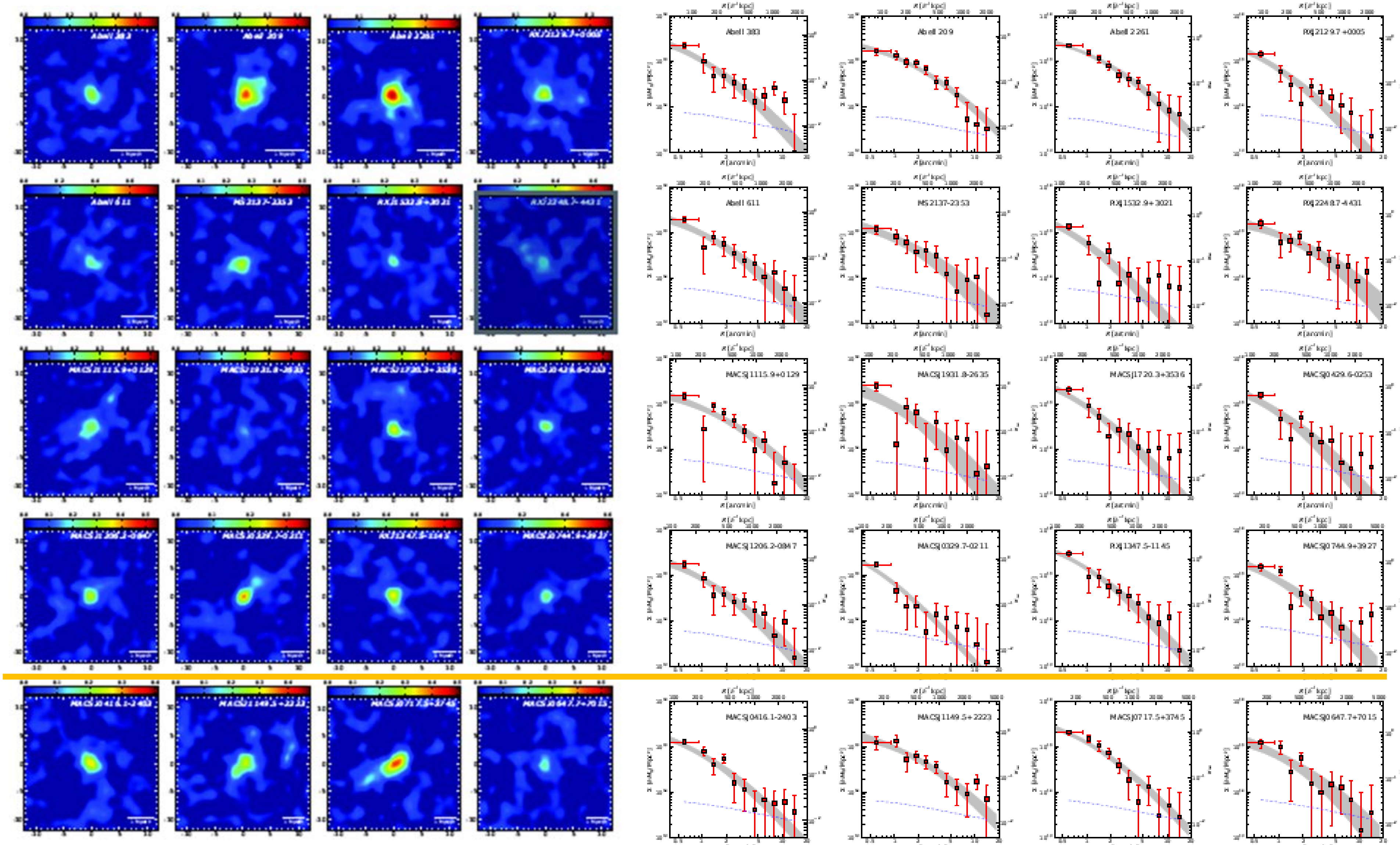

Umetsu et al. 2014, *ApJ*, 795, 163

CLASH X-ray-selected Subsample ($0.18<z<0.9$)

- **High-mass clusters with smooth X-ray morphology**
  - T_x > 5keV (M_{200} > 5e14M_{sun}/h)
  - Small BCG to X-ray-peak offset, σ_{off} ~ 10kpc/h
  - Smooth regular X-ray morphology

    → Optimized for radial-profile analysis

- **CLASH theoretical predictions** (Meneghetti+14)
  - Composite relaxed (70%) and unrelaxed (30%) clusters
  - Mean $<c_{200}>=3.9$, $c_{200}=[3, 6]$
  - Small scatter in c_{200} : $\sigma(\ln c_{200}) = 0.16$
  - Largely free of orientation bias (~2% in $<M_{3D}>$)
  - >90% of CLASH clusters to have strong-lensing features

CLASH: Joint Analysis of Strong-lensing, Weak-lensing Shear and Magnification Data for 20 CLASH Galaxy Clusters

Umetsu et al. 2015b

(to be submitted by July 17)

Joint Analysis of Multi-probe Lensing Profiles

$$\{M_{2\mathrm{D},i}\}_{i=1}^{N_{\mathrm{SL}}}, \{\langle g_{+,i}\rangle\}_{i=1}^{N_{\mathrm{WL}}}, \{\langle n_{\mu,i}\rangle\}_{i=1}^{N_{\mathrm{WL}}}.$$

Inner *HST* strong-lensing constraints on $M_{2D}(<R)$ (Zitrin et al 15)

Strong-lensing integration radii:

$\Delta = 10''(R_{Ein}/22'')^{1/2}(N/17)^{-1/2}$ sampling, $R_{max} \sim 2\langle R_{Ein}\rangle \sim 40''$

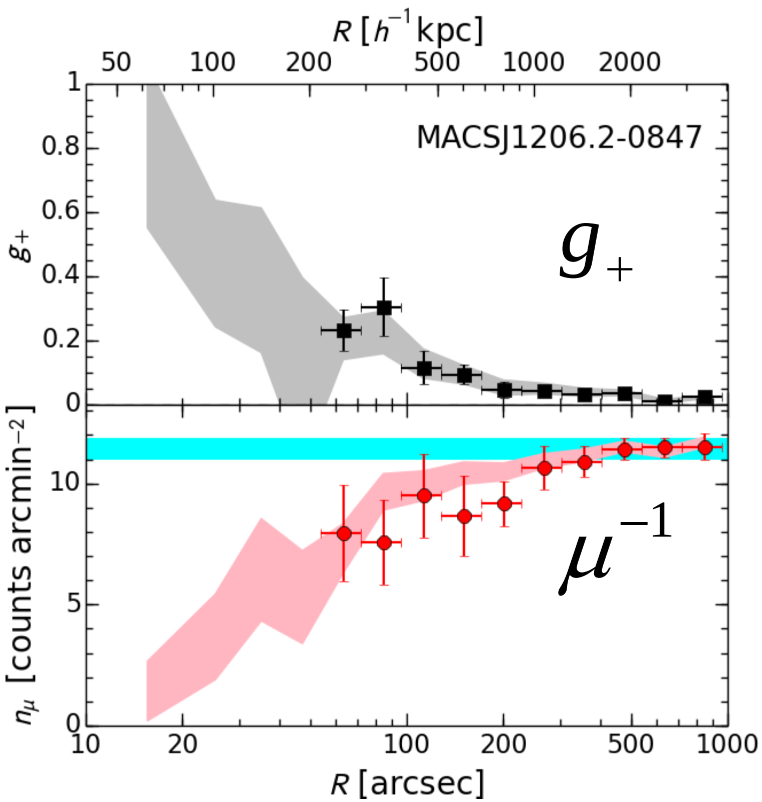

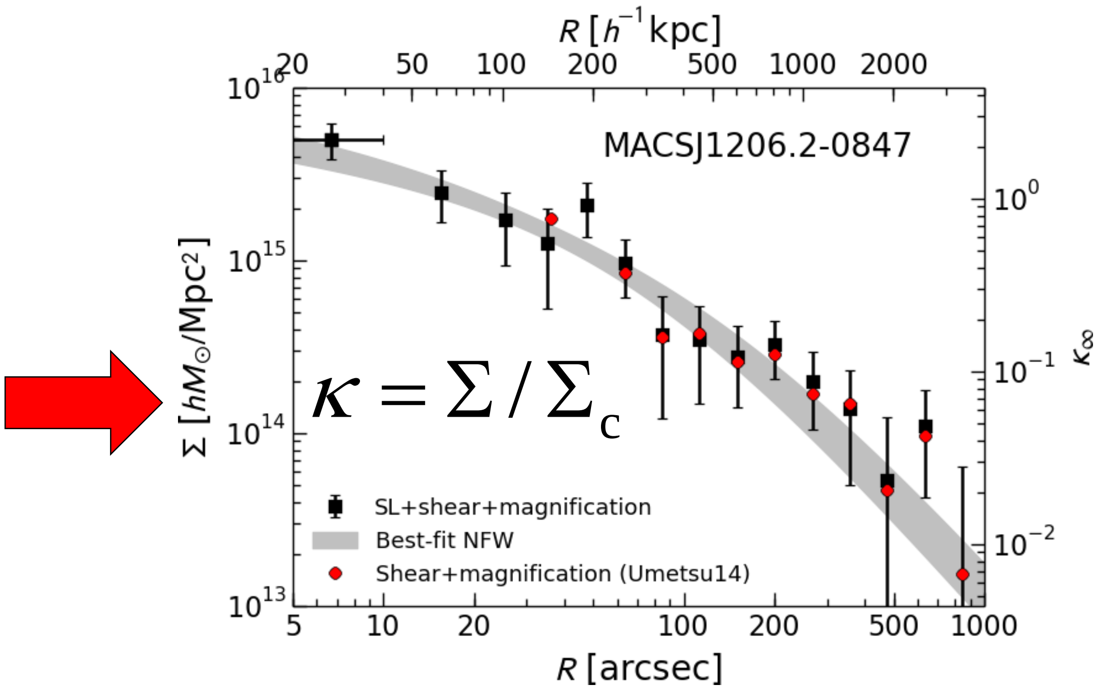

$\langle\chi^2/\mathrm{dof}\rangle$ = 0.95 for 20 CLASH clusters

CLASH Stacked Full-lensing Analysis of the X-ray-selected Subsample

Umetsu et al. 2015b

Averaged Halo Density Profile $\Sigma(R)$

Stacking lensing signals of individual clusters by

$$\langle\langle \mathbf{\Sigma} \rangle\rangle = \left(\sum_n \mathcal{W}_n\right)^{-1} \left(\sum_n \mathcal{W}_n \mathbf{\Sigma}_n\right),$$

Summing over clusters (n=1, 2, ..)

with individual “sensitivity” matrix

$$(\mathcal{W}_n)_{ij} \equiv \Sigma_{(\mathrm{c},\infty)n}^{-2} \left(C_n^{-1}\right)_{ij},$$

defined with total covariance matrix

$$C = C^{\mathrm{stat}} + C^{\mathrm{sys}} + C^{\mathrm{lss}} + C^{\mathrm{int}},$$

With “trace-approximation”, averaging (stacking) is interpreted as

$$\langle\langle M_\Delta \rangle\rangle = \frac{\sum_n \mathrm{tr}(\mathcal{W}_n)\, M_{\Delta,n}}{\sum_n \mathrm{tr}(\mathcal{W}_n)}$$

Umetsu et al. 2014, *ApJ*, 795, 163

Ensemble-averaged Error Budget

Diagonal elements (C_{ii}) averaged over all CLASH clusters

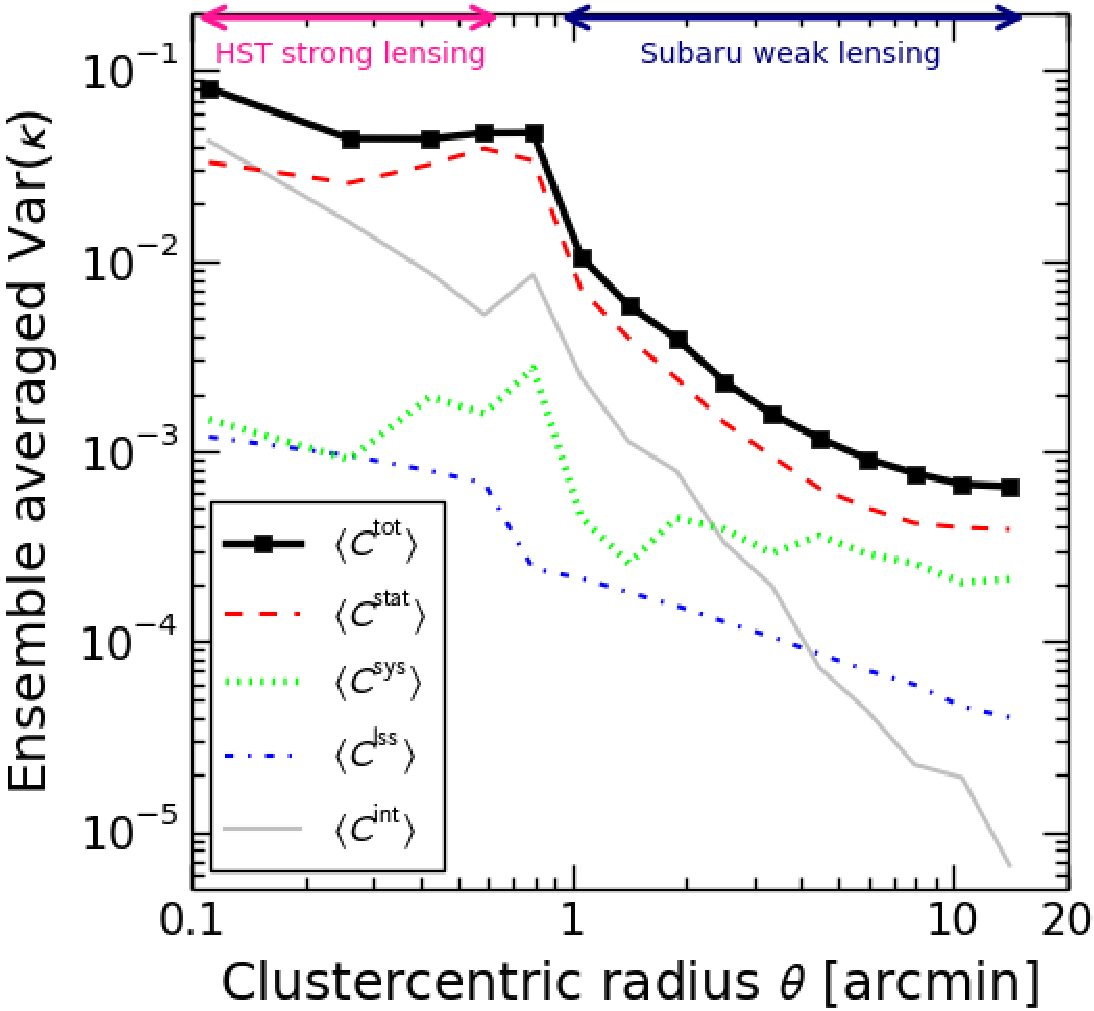

Residual mass-sheet uncertainty (Umetsu+14)

$$(C_{\rm sys})_{ii} \sim \text{const.} \sim (0.02)^2$$

Intrinsic profile variations due to triaxiality, substructure, and *c*-*M* scatter (Gruen+15)

$$(C_{\rm int})_{ii} \approx (0.2)^2 \kappa_i^2$$

Ensemble-averaged Surface Mass Density Profile

$$\Sigma(R\,|\,M) = \int \overline{\rho}\,\xi_{\rm hm}(\mathbf{r}\,|\,M)\,dx_{\parallel}$$

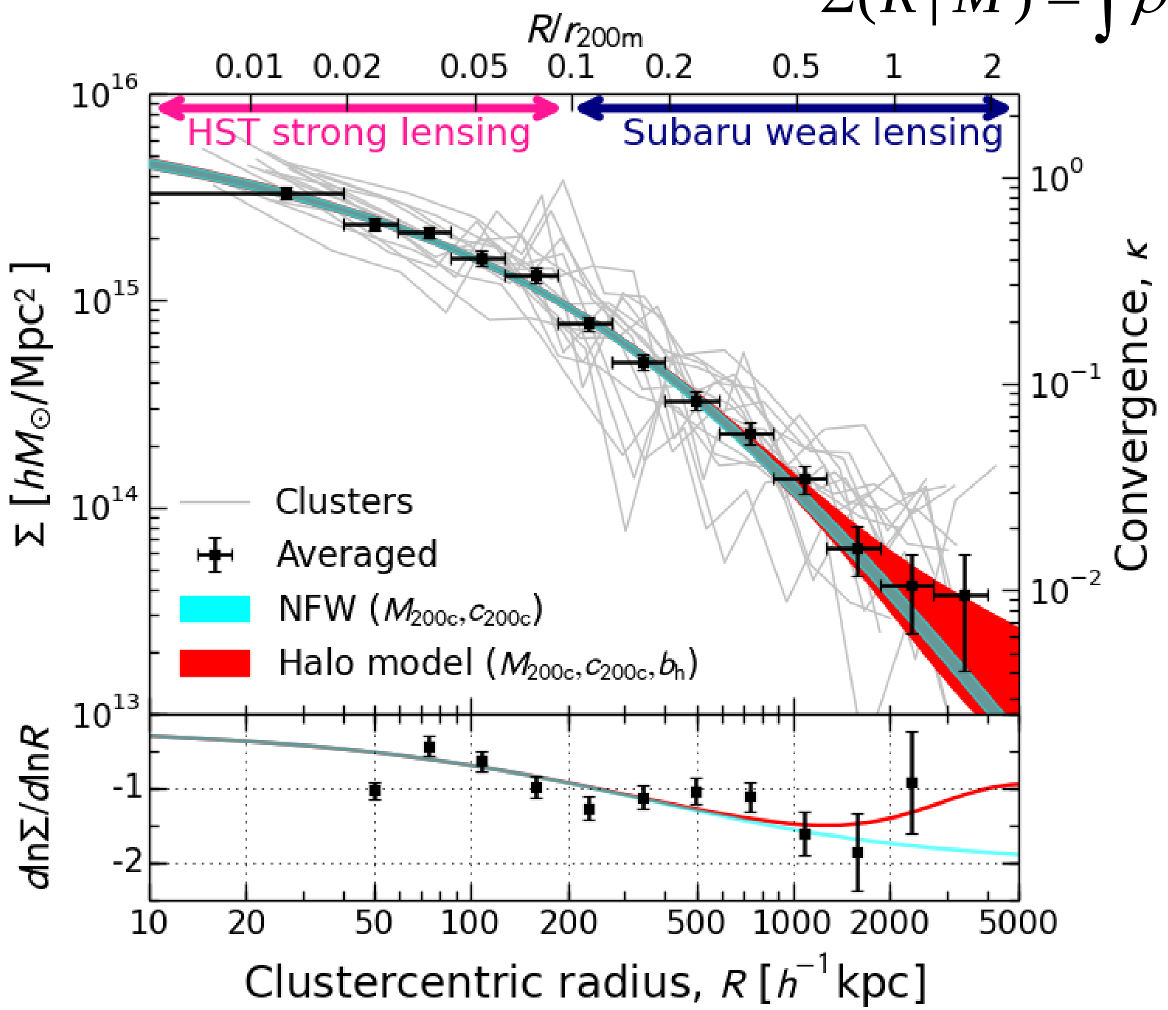

33σ detection of the ensemble-averaged mass profile out to ~$2r_{200m}$

Characterizing the Averaged Mass Profile Shape

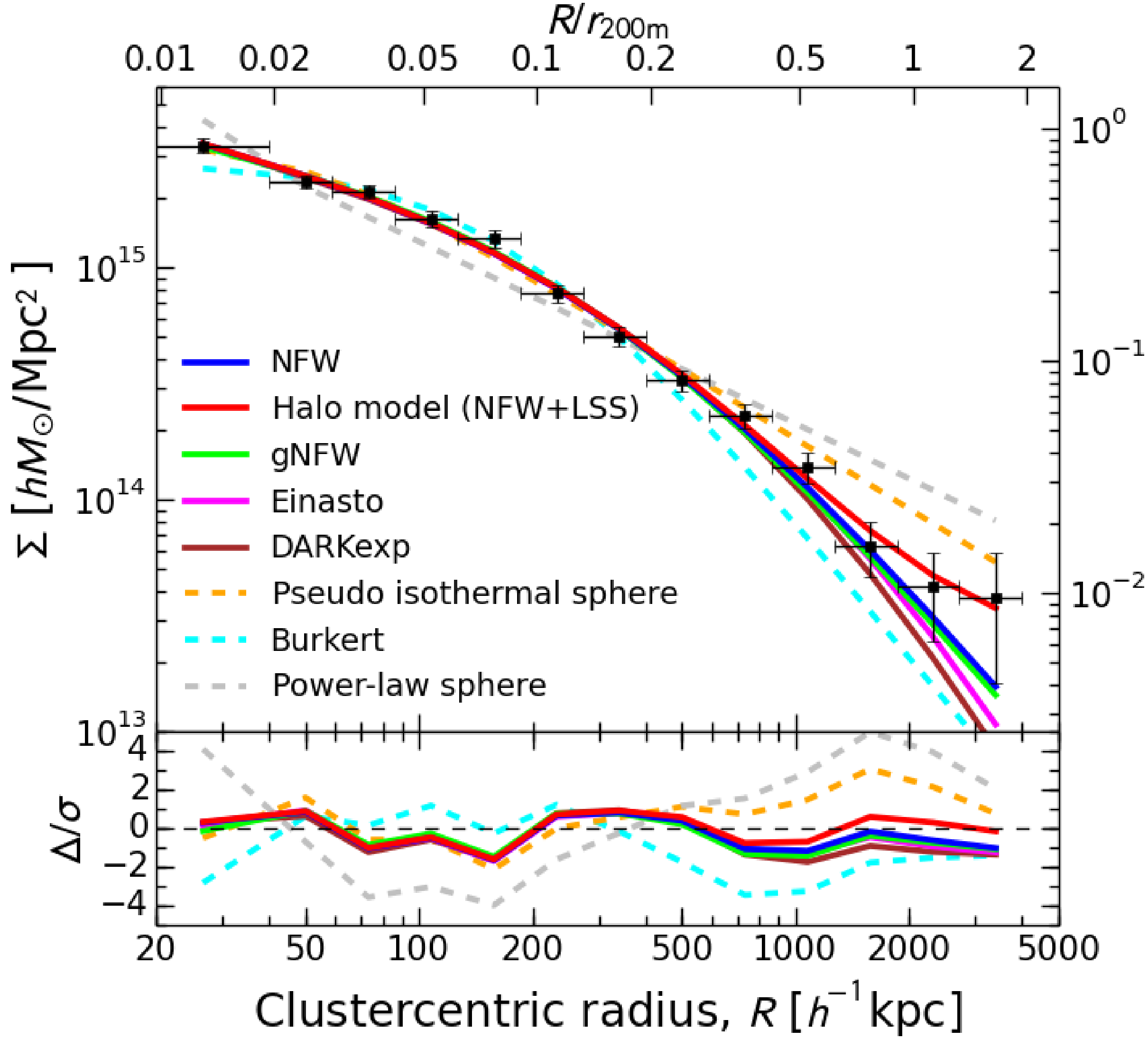

$$\Sigma(R) = \int dl\, \Delta\rho(r),$$

Models:

1. **No 2-halo term, no truncation** (f_t=1, ρ_{2h}=0)
2. **With 2-halo term (Tinker+10)**

$$\Delta\rho(r) = f_t(r)\, \rho_h(r) + \rho_{2h}(r),$$

$$f_t(r) = \left[1 + \left(\frac{r}{r_t}\right)^2\right]^{-2},$$

Comparison of Best-fit Models

Acceptable fits: *p* values (PTE) > 0.05

Table 4
Best-fit models for the stacked mass profile of the CLASH X-ray-selected subsample

Model	M_{200c} ($10^{14} M_\odot\, h_{70}^{-1}$)	c_{200c}	Shape/structural parameters	b_h	χ^2/dof	PTE[a]	Notes
NFW	$14.4^{+1.1}_{-1.0}$	$3.76^{+0.29}_{-0.27}$	$\gamma_c = 1$	—	11.3/11	0.419	No truncation
gNFW	$14.1^{+1.1}_{-1.1}$	$4.04^{+0.53}_{-0.52}$	$\gamma_c = 0.85^{+0.22}_{-0.31}$	—	10.9/10	0.366	No truncation
Einasto	$14.7^{+1.1}_{-1.1}$	$3.53^{+0.36}_{-0.39}$	$\alpha_E = 0.232^{+0.042}_{-0.038}$	—	11.7/10	0.306	No truncation
DARKexp–γ[b]	$14.5^{+1.2}_{-1.1}$	$3.53^{+0.42}_{-0.42}$	$\phi_0 = 3.90^{+0.41}_{-0.45}$	—	13.5/10	0.198	No truncation
Pseudo isothermal	—	—	$V_c = 1762^{+40}_{-39}$ km/s, $r_c = 69^{+7}_{-7}$ kpc	—	23.6/11	0.015	No truncation
Burkert	$11.6^{+0.8}_{-0.8}$	—	$r_{200c}/r_0 = 8.81^{+0.42}_{-0.41}$	—	29.9/11	0.002	No truncation
Power-law sphere	$12.5^{+0.8}_{-0.8}$	—	$\gamma_c = 1.78^{+0.02}_{-0.02}$	—	93.5/11	0.000	No truncation
Halo model[c]:							
NFW+LSS (i)	$14.1^{+1.0}_{-1.0}$	$3.79^{+0.30}_{-0.28}$	$\gamma_c = 1$	9.3	10.9/11	0.450	ΛCDM $b_h(M)$ scaling
NFW+LSS (ii)	$14.4^{+1.4}_{-1.3}$	$3.74^{+0.33}_{-0.30}$	$\gamma_c = 1$	$7.4^{+4.6}_{-4.7}$	10.8/10	0.377	b_h as a free parameter
Einasto+LSS (i)	$14.3^{+1.1}_{-1.1}$	$3.69^{+0.36}_{-0.42}$	$\alpha_E = 0.248^{+0.051}_{-0.047}$	9.3	10.7/10	0.385	ΛCDM $b_h(M)$ scaling
Einasto+LSS (ii)	$14.5^{+1.9}_{-1.6}$	$3.65^{+0.47}_{-0.61}$	$\alpha_E = 0.245^{+0.061}_{-0.053}$	$8.7^{+5.3}_{-5.6}$	10.6/9	0.301	b_h as a free parameter
DARKexp+LSS (i)	$14.2^{+1.2}_{-1.1}$	$3.64^{+0.44}_{-0.46}$	$\phi_0 = 3.89^{+0.51}_{-0.54}$	9.3	11.7/10	0.308	ΛCDM $b_h(M)$ scaling
DARKexp+LSS (ii)	$14.0^{+1.8}_{-1.6}$	$3.69^{+0.53}_{-0.57}$	$\phi_0 = 3.85^{+0.57}_{-0.61}$	$10.1^{+4.9}_{-5.1}$	11.6/9	0.235	b_h as a free parameter

[a] Probability to exceed the observed χ^2 value.
[b] We use Dehnen–Tremaine γ-models with the central cusp slope $\gamma_c = 3\log_{10}\phi_0 - 0.65$ $(1.7 \le \phi_0 \le 6)$ as an analytic fitting function for the DARKexp density profile.
[c] For halo model predictions, we decompose the total mass overdensity $\Delta\rho(r) = \rho(r) - \overline{\rho}_m$ as $\Delta\rho = f_t\rho_h + \rho_{2h}$ where $\rho_h(r)$ is the halo density profile, $\rho_{2h}(r) = \overline{\rho}_m b_h \xi_m^L(r)$ is the two-halo term, and $f_t(r) = (1 + r^2/r_t^2)^{-2}$ describes the steepening of the density profile in the transition regime around the truncation radius r_t, which is assumed to be $r_t = 3r_{200c}$.

- Consistent with cuspy density profiles (NFW, Einasto, DARKexp)
- Cuspy models that include ΛCDM 2-halo term (b_h~9.3) give improved fits
- The best model reproduces the observed Einstein radius, R_{Ein}~ 20” at z_s=2

Einasto Shape Parameter

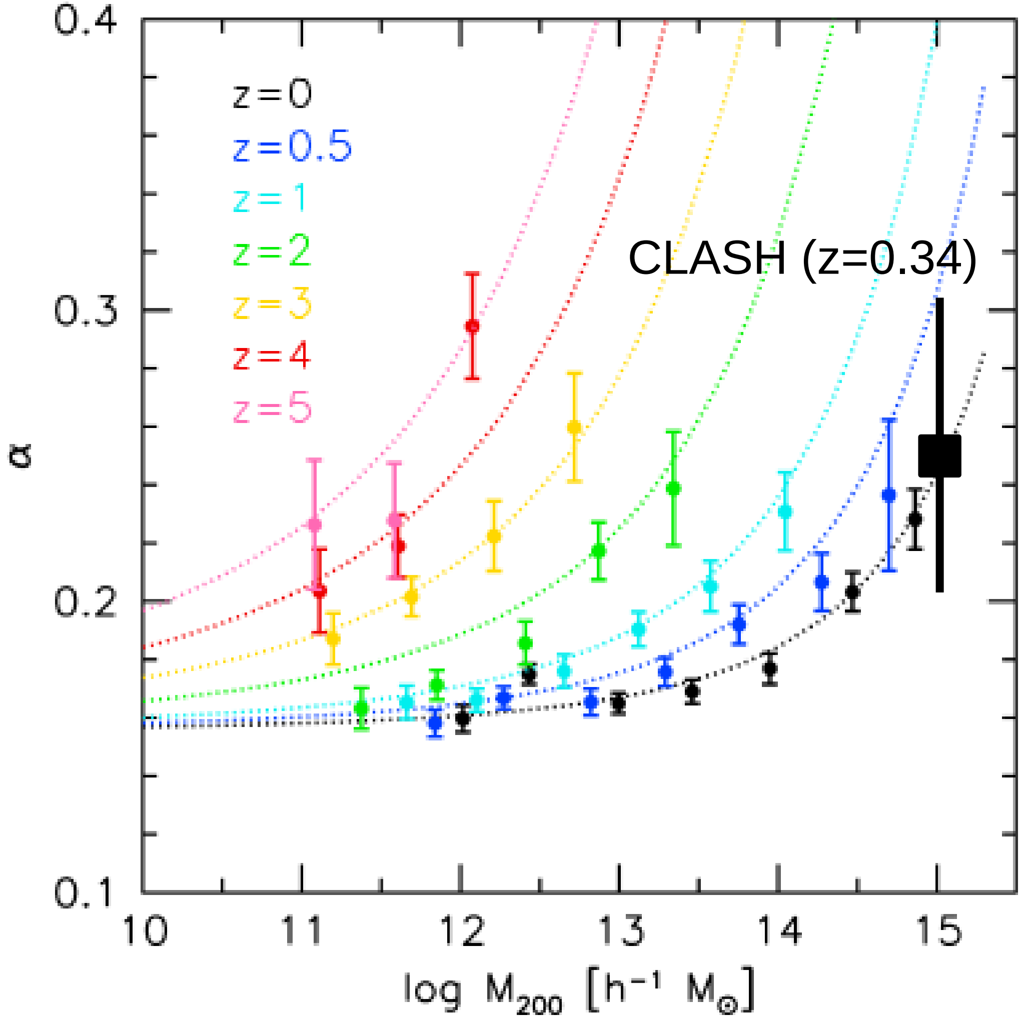

Einasto+LSS model

$$\alpha_E = 0.248^{+0.051}_{-0.047}$$

$$M_{200c} \approx 10^{15} M_{sun}/h,$$

$$c_{200c} \approx 3.7\ (c_{vir} \sim 5)$$

$$z = 0.34$$

Einasto Shape Parameter

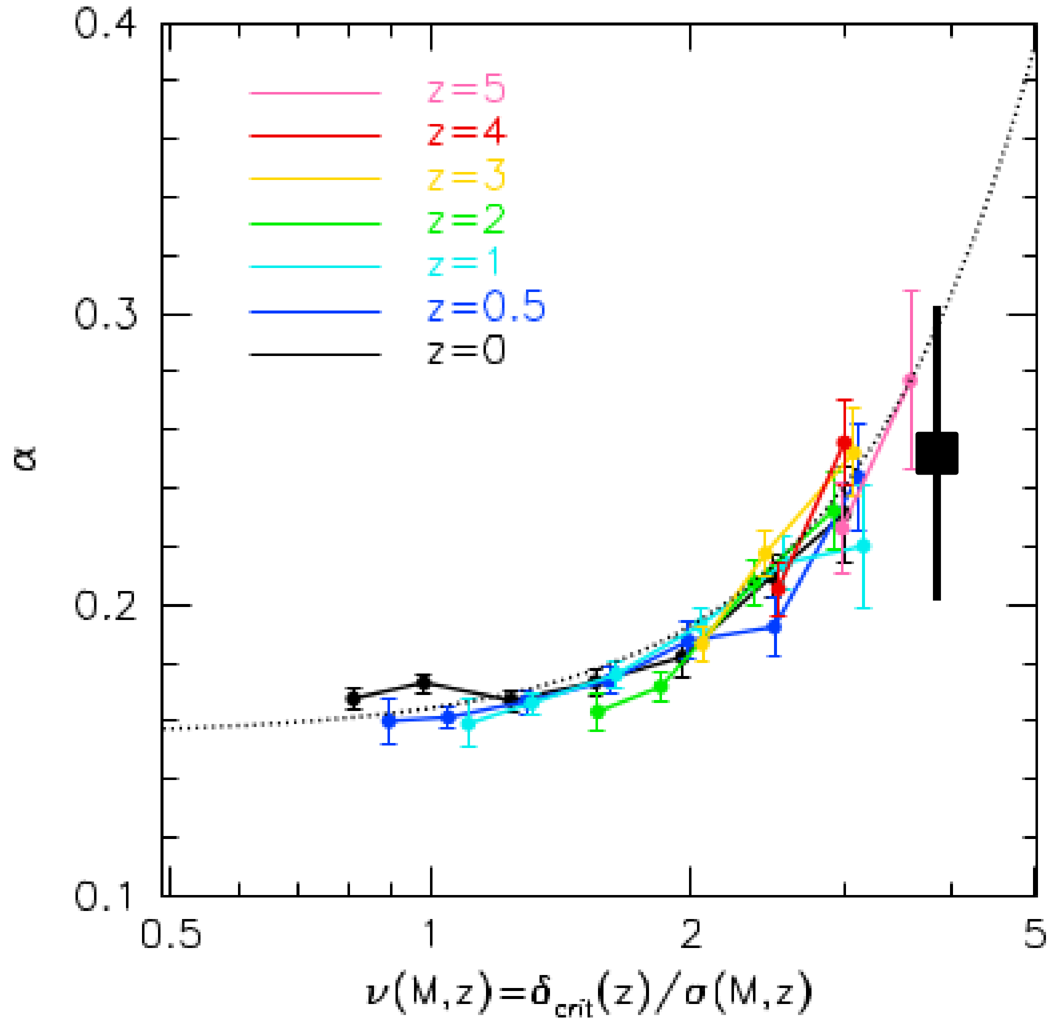

Einasto+LSS model

$$\alpha_E = 0.248^{+0.051}_{-0.047}$$

$$M_{200c} \approx 10^{15} M_{sun}/h,$$

$$c_{200c} \approx 3.7\ (c_{vir} \sim 5)$$

$$z = 0.34$$

Interpreting Effective Halo Mass

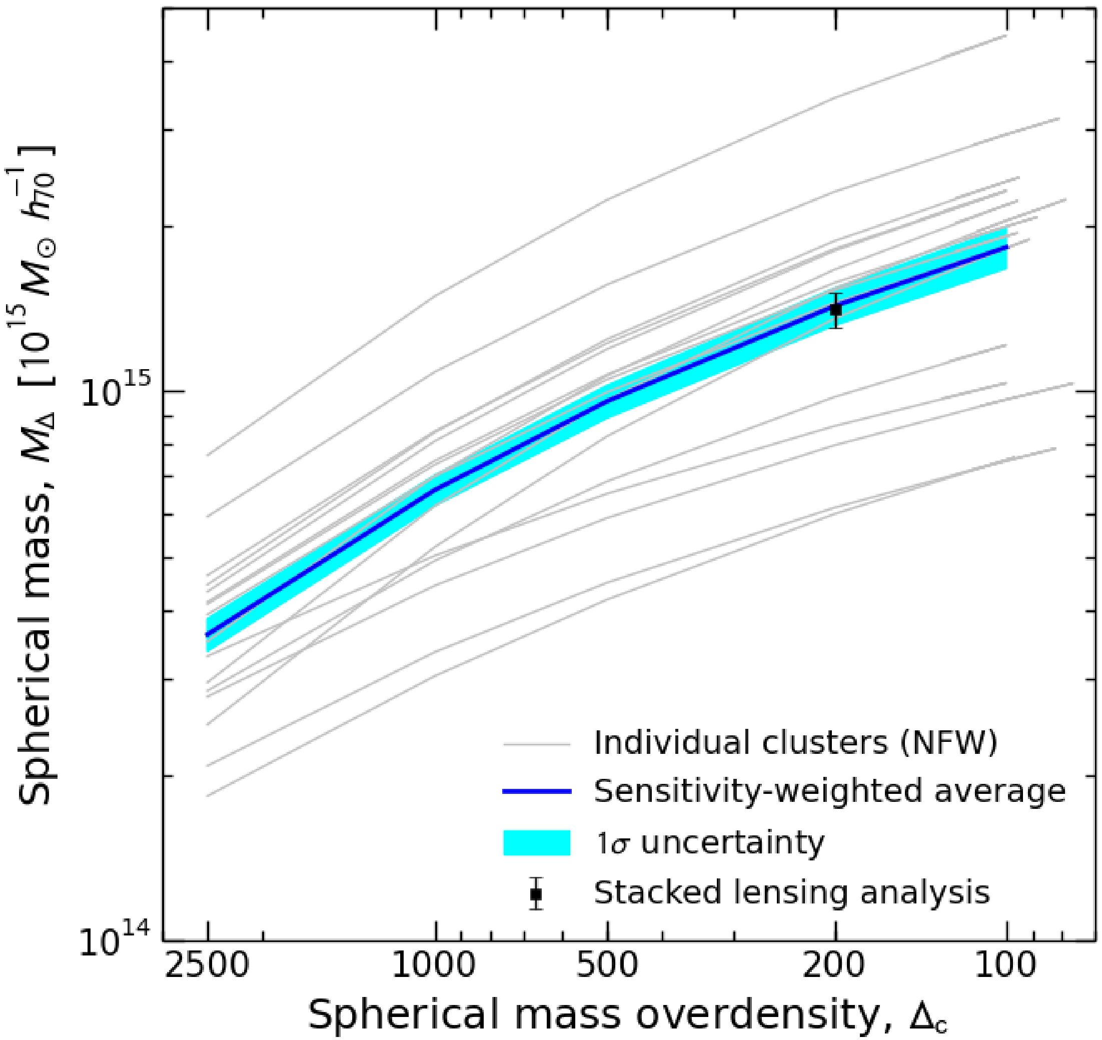

Sensitivity-weighted composite-halo profile (Umetsu+14)

$$\langle\langle M_\Delta \rangle\rangle = \frac{\sum_n \mathrm{tr}(\mathcal{W}_n)\, M_{\Delta,n}}{\sum_n \mathrm{tr}(\mathcal{W}_n)}$$

$$(\mathcal{W}_n)_{ij} \equiv \Sigma^{-2}_{(\mathrm{c},\infty)n} \left(C_n^{-1}\right)_{ij}$$

CLASH Concentration-Mass Relation for the X-ray-selected Subsample

Umetsu et al. 2015b

CLASH *c*-*M* Scaling Relation

Consider a power-law scaling relation of the form:

$$c_{200c} = 10^{\alpha} \left(\frac{M_{200c}}{M_{\rm piv}} \right)^{\beta} \left(\frac{1+z}{1+z_{\rm piv}} \right)^{\gamma},$$

with pivot mass and redshift $M_{\rm piv} = 10^{15} M_{\rm sun}/h,\ z_{\rm piv} = 0.34$

Define new independent (*X*) and dependent (*Y*) variables:

$$Y \equiv \log_{10} \left[\left(\frac{1+z}{1+z_{\rm piv}} \right)^{-\gamma} c_{200c} \right],$$

$$X \equiv \log_{10} \left(M_{200c}/M_{\rm piv} \right).$$

$$Y = \alpha + \beta X$$

Redshift slope is fixed to the theoretical prediction for the CLASH sample, γ=-0.668 (Meneghetti+14)

Bayesian Regression Analysis

We take into account

- Covariance between observed *M* and *c*
- Intrinsic scatter in *c*
- Non-uniformity in mass probability distribution *P*(log*M*)

Conditional probability *P*(*y*|*x*): (*x*,*y*) = observed (*X*,*Y*)

$$\ln \mathcal{P}(\boldsymbol{y}|\boldsymbol{x}) = -\frac{1}{2}\sum_n \left[\ln\left(2\pi\sigma_n^2\right) + \left(\frac{y_n - \langle y_n|x_n\rangle}{\sigma_n}\right)^2\right], \quad (35)$$

where $\langle y_n|x_n\rangle$ and $\sigma_n^2 \equiv \mathrm{Var}(y_n|x_n)$ are the conditional mean and variance of y_n given x_n, respectively:

$$\langle y_n|x_n\rangle = \alpha + \beta\mu + \frac{\beta\tau^2 + C_{xy,n}}{\tau^2 + C_{xx,n}}(x_n - \mu),$$

$$\sigma_n^2 = \beta^2\tau^2 + \sigma_{Y|X}^2 + C_{yy,n} - \frac{(\beta\tau^2 + C_{xy,n})^2}{\tau^2 + C_{xx,n}}, \quad (36)$$

where $\sigma_{Y|X}$ is the intrinsic scatter in the Y–X relation;

Marginalized Posterior Distributions

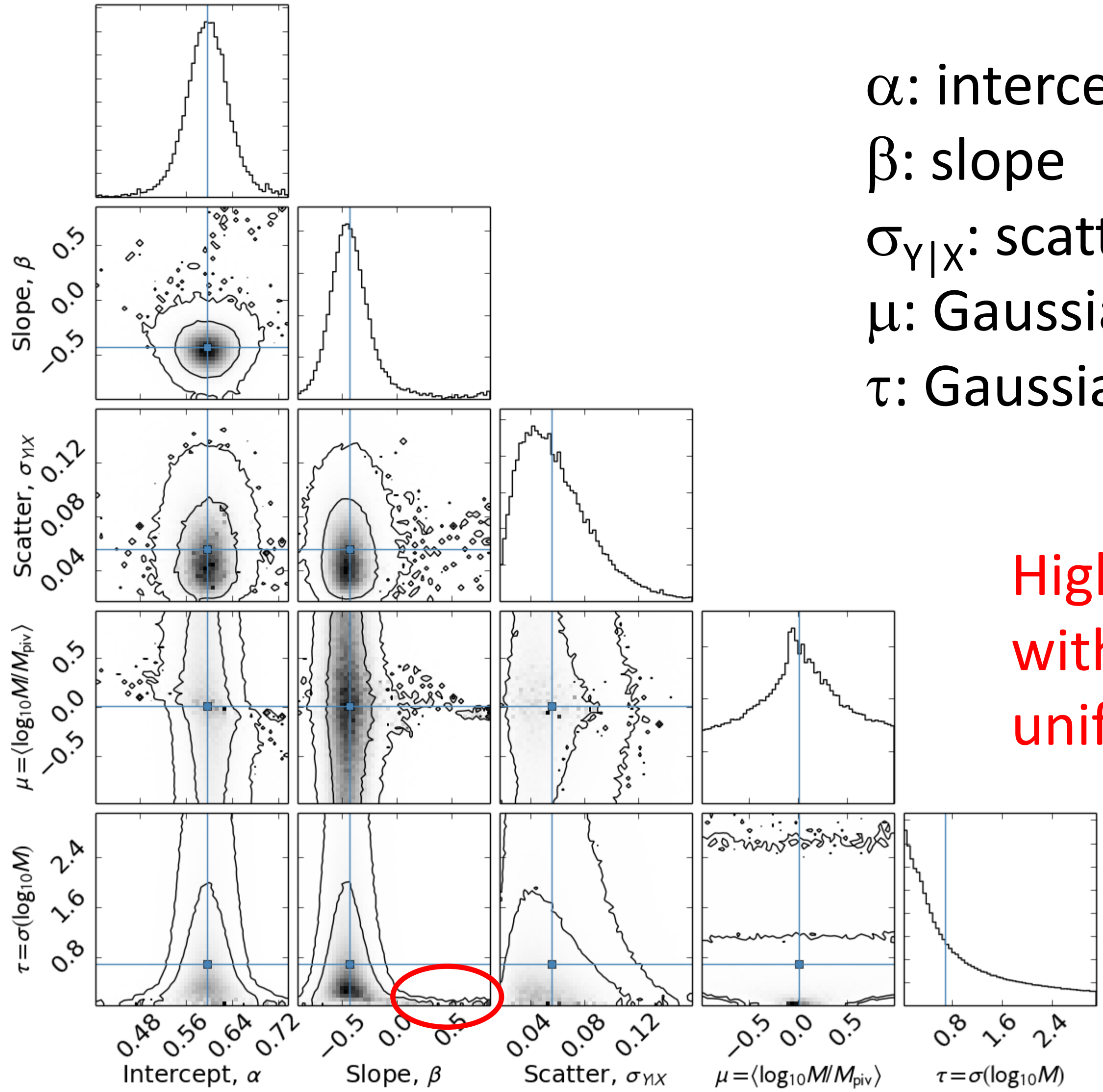

α: intercept

β: slope

$\sigma_{Y|X}$: scatter

μ: Gaussian mean of $P(\ln M)$

τ: Gaussian width of $P(\ln M)$

High β tail associated with small τ: i.e., non-uniform $P(\ln M)$

Observations vs. Predictions

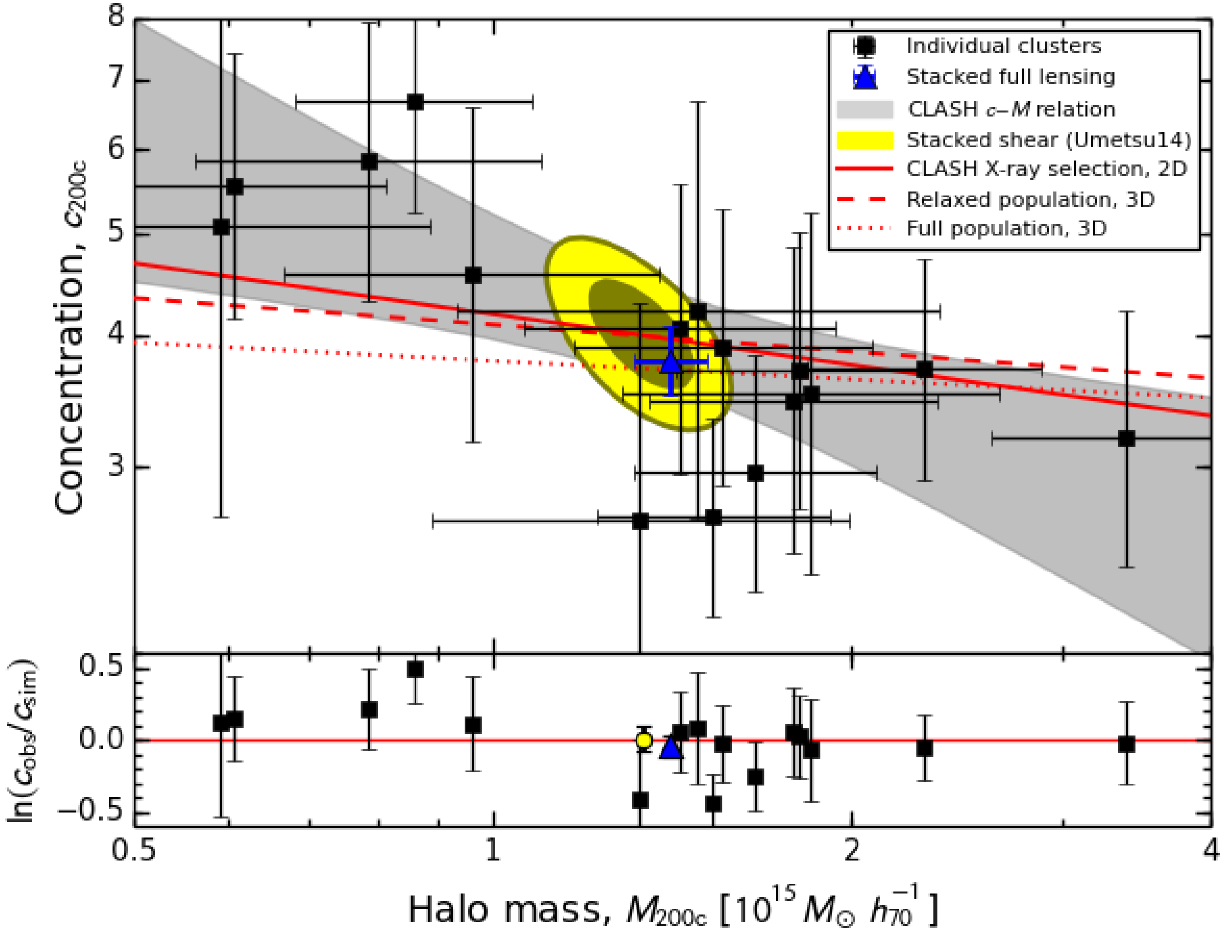

Normalization, slope, & scatter are all consistent with LCDM when the CLASH selection function based on X-ray morphological regularity and the projection effects are taken into account

Comparison with LCDM Models

Table 5
Comparison of measured and predicted concentrations for the CLASH X-ray-selected subsample

Author	Sample	3D/2D	Function[a]	$c^{(\rm obs)}/c^{(\rm pred)}$ Average[c]	σ[d]	χ^2	PTE[b]
Theory:							
Duffy et al. (2008)	full	3D	c–M	1.331 ± 0.108	0.334	22.6	0.046
Duffy et al. (2008)	relaxed	3D	c–M	1.165 ± 0.094	0.290	13.6	0.399
Prada et al. (2012)	full	3D	c–ν	0.733 ± 0.065	0.244	24.6	0.026
Bhattacharya et al. (2013)	full	3D	c–ν	1.169 ± 0.095	0.292	14.1	0.369
Bhattacharya et al. (2013)	relaxed	3D	c–ν	1.131 ± 0.092	0.277	12.4	0.494
Dutton & Macciò (2014)	full	3D	c–M	1.061 ± 0.086	0.262	10.4	0.659
Meneghetti et al. (2014)	full	3D	c–M	1.061 ± 0.089	0.279	10.2	0.675
Meneghetti et al. (2014)	relaxed	3D	c–M	0.990 ± 0.083	0.249	9.2	0.760
Diemer & Kravtsov (2015)	full (median)	3D	c–ν	1.021 ± 0.083	0.330	14.4	0.349
Diemer & Kravtsov (2015)	full (mean)	3D	c–ν	1.060 ± 0.086	0.326	13.8	0.391
Meneghetti et al. (2014)	full	2D	c–M	1.087 ± 0.092	0.336	13.5	0.413
Meneghetti et al. (2014)	relaxed	2D	c–M	1.040 ± 0.086	0.283	10.8	0.628
Meneghetti et al. (2014)	CLASH	2D	c–M	0.988 ± 0.078	0.227	9.6	0.730
Observations:							
Merten et al. (2015)	CLASH	2D	c–M	1.133 ± 0.087	0.209	9.2	0.754

[a] c–M: power-law $c(M, z)$ relation; c–ν: halo concentration given as a function of peak height $\nu(M, z)$.
[b] Probability to exceed the measured χ^2 value assuming the standard χ^2 probability distribution function.
[c] Weighted geometric average of observed-to-predicted concentration ratios.
[d] Standard deviation of the distribution of observed-to-predicted concentration ratios.

WMAP3

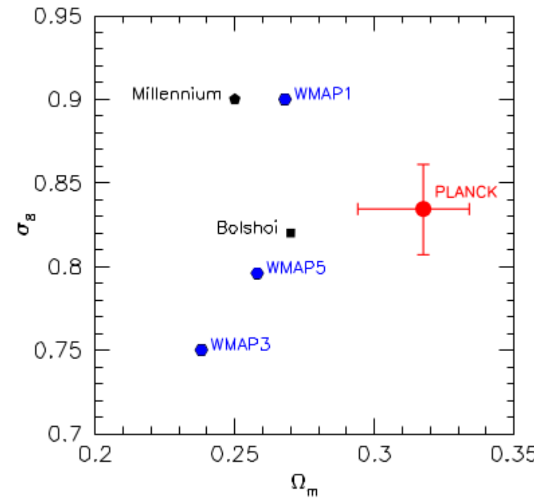

- Consistent with models that are calibrated for more recent cosmologies (WMAP7 and later)
- Better agreement is achieved when selection effects (overall degree of relaxation) are taken into account

Ensemble Calibration of Cluster Masses

Umetsu et al. 2015b

Planck13 CMB vs. Cluster Cosmology

b=0.2?? – 0.4??

- Planck: 3σ tension between SZ cluster counts and CMB cosmology
- assumes M_{Planck} / M_{true} = (1-b) = 0.8
- calibrated with XMM hydrostatic masses (Arnaud et al. 2010) + simulations

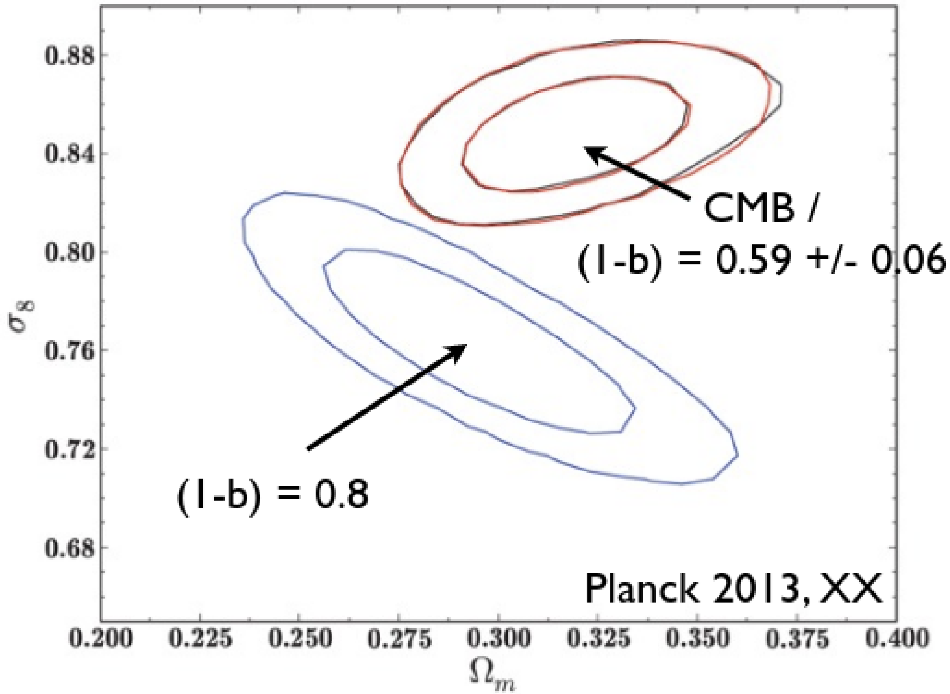

suggested explanations:

- mass bias underestimated (and no accounting for uncertainties)
- 2.9σ detection of neutrino masses: Σm_ν = (0.58 +/- 0.20) eV (Planck+WMAPpol+ACT+BAO: Σm_ν < 0.23 eV, 95% CL)

Slide taken from Anja von der Linden's presentation

Comparison with *Planck* Masses: *It's not so simple!!!*

Mass-dependent bias (20-45%) observed for *Planck* mass estimates

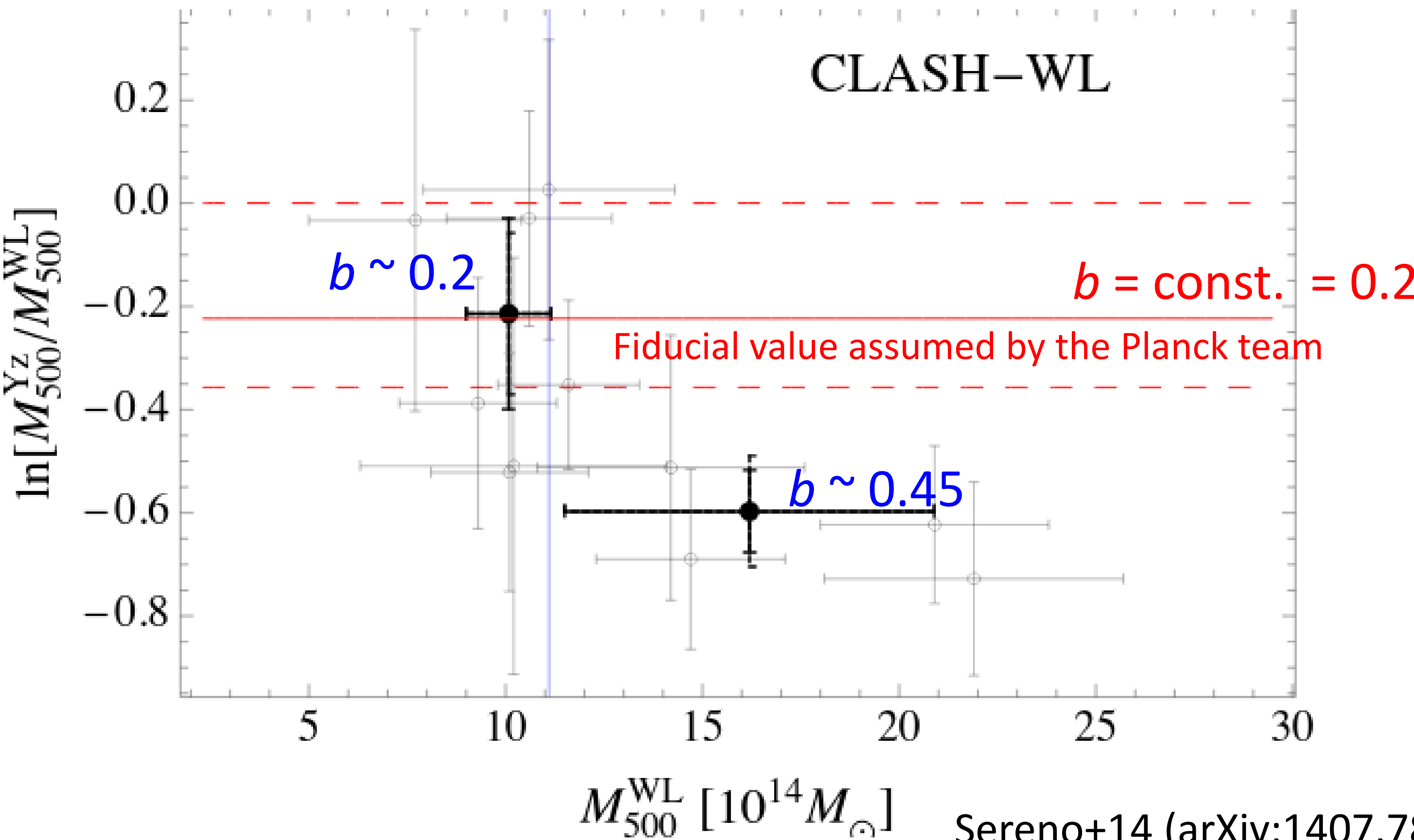

Sereno+14 (arXiv:1407.7869)

CLASH Internal Consistency

M(<*r*) de-projected assuming spherical NFW density profiles

$$\left\langle \frac{M_{3D}(\mathrm{WL+SL})}{M_{3D}(\mathrm{WL})} \right\rangle$$

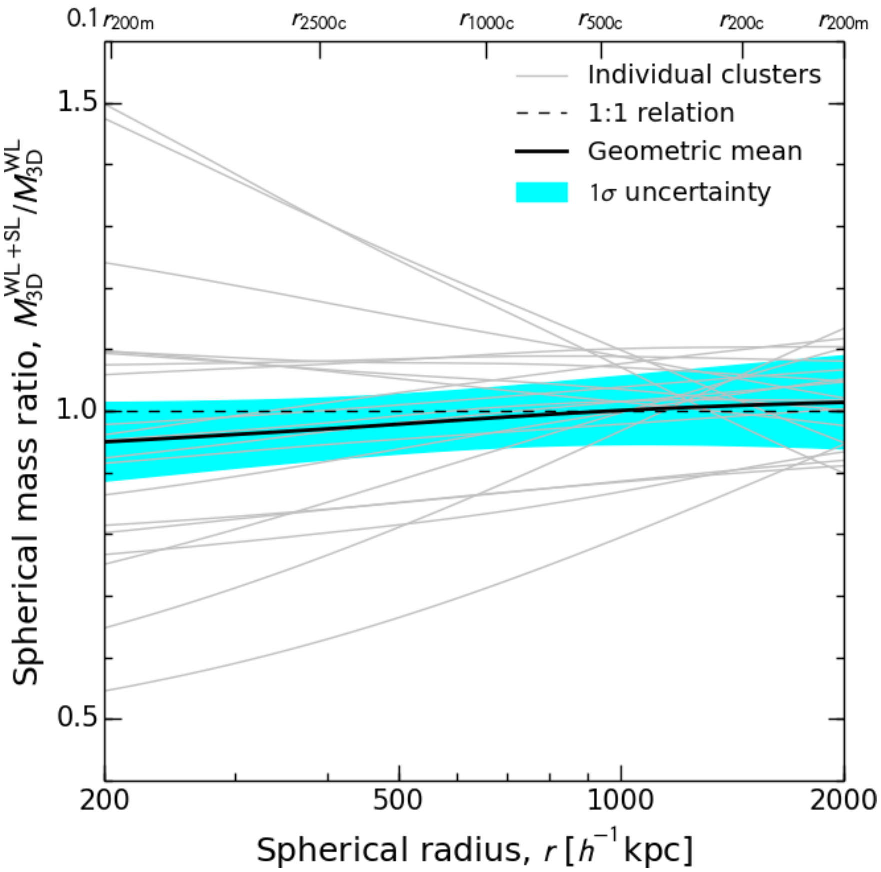

Internal systematic uncertainty in the overall mass calibration, empirically derived to be < 5% +/- 6%

Comparisons with Other Surveys

Weighing the Giants
(Stanford)

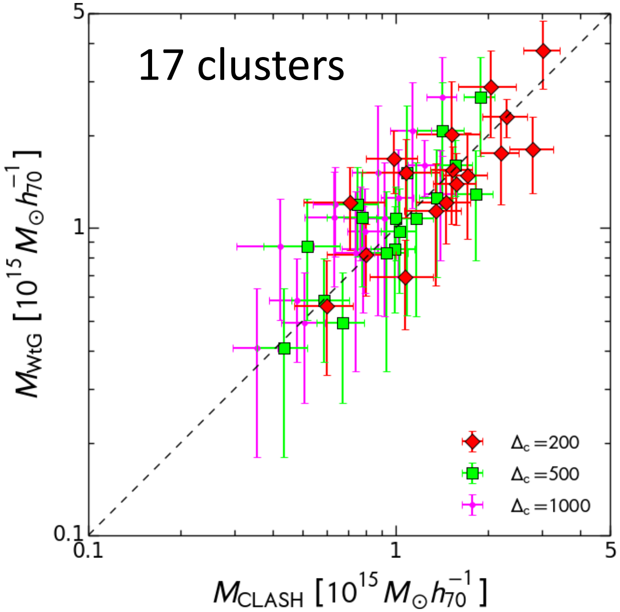

LoCuSS
(Okabe & Smith 15)

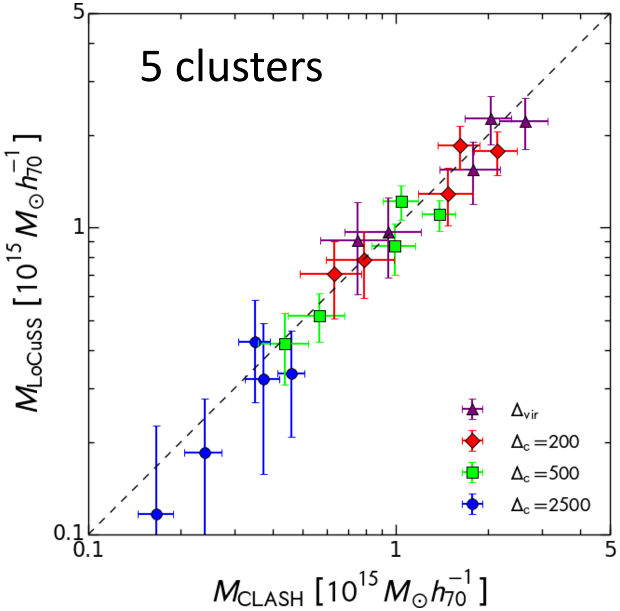

CCCP (Hoekstra+15)

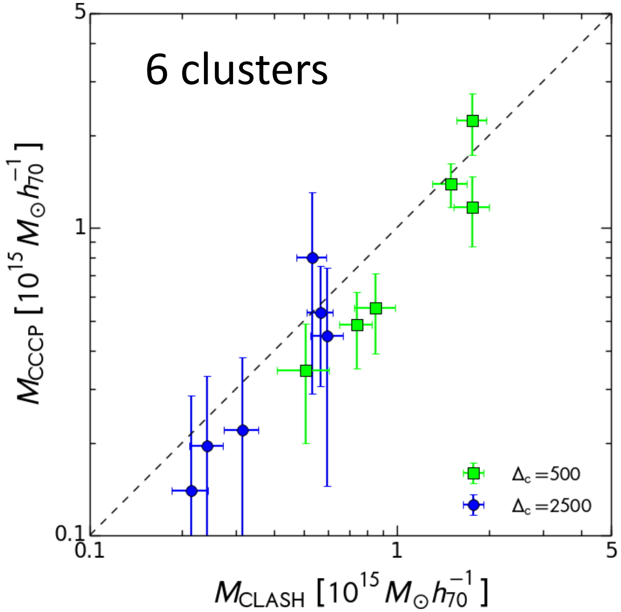

Summary

- Ensemble-averaged mass profile shape
  - Data favor cuspy density profiles predicted for collisionless-DM-dominated halos in gravitational equilibrium (NFW, Einasto, DARKexp)
  - The highest-ranked model is the 2-parameter NFW+LSS model including the 2-halo term using the LCDM *b*-*M* relation ($b_h \sim 9.3$)
  - c_{200c} = 3.8 +/- 0.3 at $M_{200c}=10^{15}M_{sun}/h$, z=0.34
- Concentration vs. mass relation
  - Fully consistent with LCDM when the CLASH selection function based on X-ray morphological regularity and the projection effects are taken into account
- Mass calibration
  - Internal consistency better than 5% +/- 6% by comparison with the WL-only analysis of Umetsu et al. (2014)

Future/ongoing Work

- Calibrating Planck SZE cluster masses using the CLASH mass measurements
- Characterization of individual cluster Σ profiles
  - Mass dependence of Einasto shape parameter
  - Inner density slopes vs. cluster properties
- Testing modified gravity models (e.g., Narikawa & Yamamoto 12)
- Comparison with dynamical Jeans analyses from the CLASH-VLT survey (e.g., Biviano et al. 13)

CLASH Products released

http://archive.stsci.edu/prepds/clash/

- Calibrated and co-added images [HST, Subaru]
- Object catalogs [HST, Subaru]